FERROMAGNETIC RESONANCE OF PRECIPITATED PHASES IN NATURAL GLASSES

David L. GRISCOM

Naval Research Laboratory, Washington, DC 20375, USA

This paper describes the practical application of ferromagnetic resonance (FMR) in characterizing the iron-rich precipitates commonly occurring in natural glasses. Following a capsule introduction to the principles of FMR powder pattern analysis, some new results for obsidians and Mount St Helens ash are briefly presented. Attention is later drawn to the critical influences of gas-phase equilibria in determining the natures of the precipitated phases in fine particulate glasses, and it is demonstrated that synthetic "natural glass analogues" can be important aids in interpreting the FMR spectra of natural samples. An extensive discussion of the ferromagnetic phases in lunar glasses of both volcanic and micrometeoroid-impact origins is built largely upon elements of the author's previously published and unpublished work, and suggestions are offered for future FMR studies of these materials. Finally, an appendix compares two methods of thermomagnetic analysis based on FMR and contrasts these with the results of more classical techniques.

1. Introduction

The study of natural glasses undoubtedly holds the key to understanding many geophysical and geochemical processes on the Earth and the other terrestrial planets, including the Earth's Moon [1]. However, as emphasized by O'Keefe [1], many mysteries remain, and the unlocking of these may well depend on the steady introduction of new analytical techniques for characterizing both the available natural glass samples and their synthetic analogues.

Electron spin resonance (ESR) is a technique which is not new per se in its application to natural glasses. Extensive studies of terrestrial natural glasses were carried out to obtain a reference data base prior to the return of the first lunar samples in 1969, e.g. refs. [2] and [3]. Perhaps it was the ensuing engrossment with the lunar samples themselves which delayed further publication of these results until substantially later dates. Several post-Apollo papers have now dealt with Lybian Desert glass [4–6], tektites [5], and Fulgurites [5].

Another recent body of literature involved the application of ESR to determine oxidation–reduction equilibria of multivalent elements in silicate melts which model planetary magmas, e.g. refs. [7–14]. The results of these studies promise to be of particular importance in geochemistry and basaltic petrology [15]. However, most of the synthetic melts so far investigated cannot be considered "natural glass analogues" since glasses of these compositions are

rarely found in nature [1]. Nevertheless, the ESR methodology and data base carefully developed in refs. [7-14] should prove indispensable in future studies of paramagnetic ions dissolved in natural glasses.

The general topic of ESR in glasses has been the subject of a recent review [16]. As discussed there, it is useful to draw a distinction between *paramagnetic* resonance, due to a system of dilute, weakly interacting electron spins, and *ferromagnetic* resonance (FMR), which is encountered when ferro- or ferri-magnetic * compounds are included in the sample. While both experiments are carried out on the same ESR spectrometer, the spectral line shapes, linewidths and intensities and their temperature dependences are entirely different in the two cases. For example, whereas in paramagnetic resonance the intensity varies as the reciprocal of absolute temperature, in FMR the signal intensities can be nearly independent of temperature – or even increasing functions of tempera-ture! The use of such FMR intensity measurements as a diagnostic tool will be discussed in section 5, below. Similarly, some aspects of FMR line shape analysis relevant to the natural glass problem will be taken up in section 2, immediately following.

It can be stated with considerable confidence (though not without some risk) that there exist no *homogeneous* natural glasses which are ferromagnetic. In all known cases, the ferromagnetism which is the subject of this paper arises from fine-grained precipitates in the glass. The broad area of FMR studies of such precipitates in glasses has been reviewed briefly [17] and will be more extensively discussed in a longer manuscript in preparation [18]. The present paper confines itself to several special issues relating to *natural* glasses and presents a substantial amount of otherwise unpublished material, thus comple-menting rather than duplicating refs. [17] and [18].

2. FMR line shape analysis for spherical, single-domain particles

As developed more thoroughly elsewhere [17,18], the FMR line shapes which are encountered in glasses depend strongly on the shapes and sizes of the precipitated particles. In principle, they might also depend on whether or not the particles are clumped together. Fortunately, however, particles precipi-tated in glasses have a strong tendency to be spherical (due to surface tension) and well dispersed (due to homogeneous nucleation). Sphericity and freedom from clumping are incalculable boons to the FMR experiment, since in these events shape anisotropy and particle–particle interactions can be neglected.

The remaining interactions are the Zeeman interaction of the magnetic moment with the applied magnetic field, magnetocrystalline anisotropy (which frequently serves to fingerprint unknown ferromagnetic phases), and anisot-

---

* In the remainder of this paper no distinction will be made between materials which are ferromagnetic (all spins parallel) and those which are ferrimagnetic (some spins antiparallel). The terminologies "ferromagnetic" and "FMR" will be uniformly applied to all compounds which are characterized by net ferromagnetic moments, magnetite being an important example.
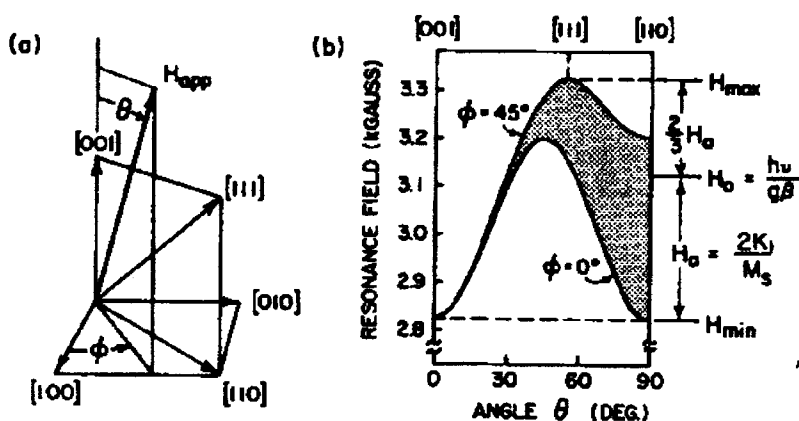
Fig. 1. Coordinate system (a) and resonance fields versus angle (b) for a spherical single crystal of a ferromagnetic mineral with cubic crystal structure and positive magnetocrystalline anisotropy constant.

ropy due to domain structure (which in the most favorable cases can be interpreted [17–19] but which more often serves to smudge the magnetocrystalline-anisotropy fingerprint). Multidomain effects will not be discussed in the present paper, except to identify certain cases where it seems likely that such effects govern the experimental line shape (see particularly, section 3).

As explained in ref. [17], the FMR experiment makes no distinction between "single domain" and "superparamagnetic" particles, single domain behavior being observed for all particles smaller than a certain diameter. For spherical particles, the single domain–multidomain threshold diameter in zero applied magnetic field is $d_0 \sim 200$ Å for metallic iron [20] and $d_0 \lesssim 480$ Å for magnetite (Fe_3O_4) [21]. However, when sufficiently large magnetic fields are applied, all domain structure is driven out regardless of particle size. The maximum applied field required to saturate a spherical particle is $H_s \equiv (4\pi/3) M_s$ [22], where M_s is saturation magnetization of the bulk material. At room temperature, the maximum saturation field for iron is $H_s \approx 7.1$ kG * while for magnetite $H_s \approx 2$ kG. Thus, if the resonance field H_{res} should substantially exceed these values, single domain behavior would be observed irrespective of particle size.

Let it be supposed that $H_{res} \gg H_s$ and that a spherical single crystal of cubic structure is available for investigation. In this case H_{res} can be expressed as a function of the angles θ and ϕ relating the direction of the applied field $\overline{H}_{app}$ to the directions of the crystallographic axes (fig. 1a). The first-order resonance

---

* Units of magnetic field used in the literature vary. Geologists have tended to favor Oersteds, while physicists, who produce their laboratory fields in an electromagnet, have preferred the unit for magnetic induction, Gauss. The currently recommended unit of magnetic induction is milli-Tesla. Note: 1 Oe = 1 G = 0.1 mT.

condition can then be stated as [23–25]

$$H_{res}(\theta,\phi) = \frac{h\nu}{g\beta} - \frac{2K_1}{M_s}\left[1 - 5\left(\cos^2\theta\,\sin^2\theta + \sin^4\theta\,\sin^2\phi\,\cos^2\phi\right)\right], \quad (1)$$

where h is Planck's constant, ν is the spectrometer frequency, g is the g factor (≈ 2), β is the Bohr magnetron, and K_1 is the first order magnetocrystalline
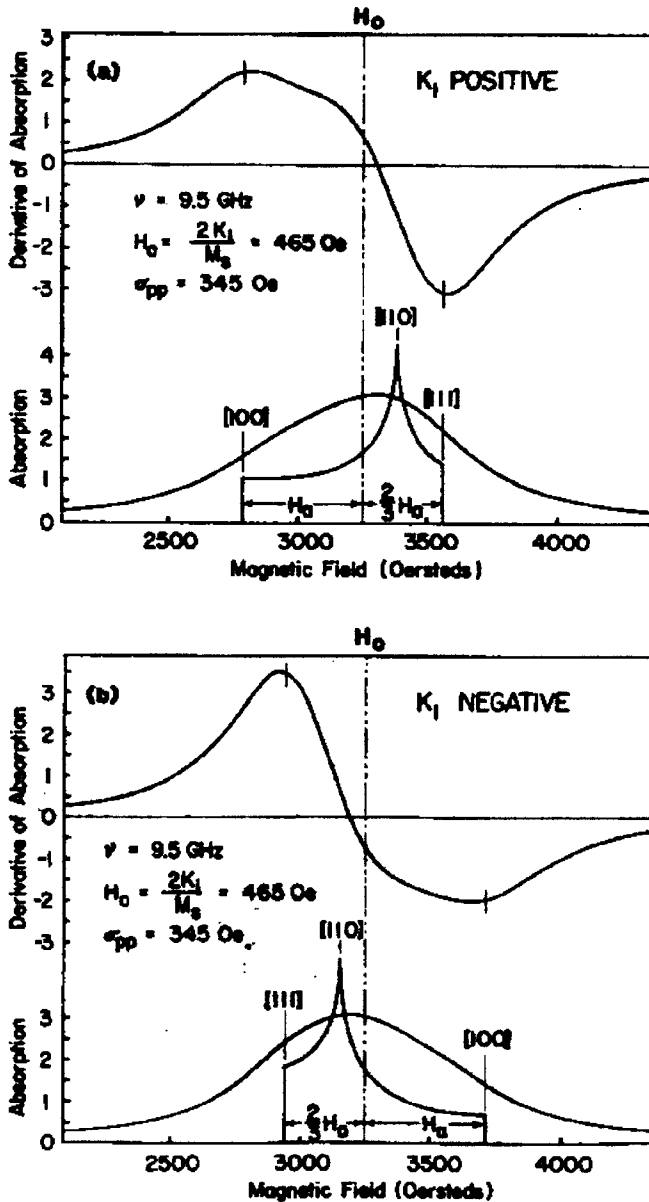

Fig. 2. FMR powder patterns, before and after convolution by a Lorentzian broadening function, for assemblies of randomly oriented, noninteracting, single-domain, spherical particles of ferromagnetic phases with cubic crystal structure. (a) $H_a > 0$, (b) $H_a < 0$. Powder patterns are below; the first derivatives of the convoluted patterns are above.

anisotropy constant. While more accurate FMR resonance conditions are available in the literature [24,26], eq. (1) is generally a good approximation and useful in any event to illustrate the general outcome of the experiment just delineated.

Fig. 1b portrays the resonance field H_{res} as a function of the angle θ for two fixed values of ϕ (0 and 45°). The shaded area between these two curves represents the range of resonance fields for all other values of ϕ. Note that for $H_a > 0$ the minimum resonance field H_{min} occurs for $\overline{H}_{app}$ parallel to [100]-type cube axes, while H_{max} occurs when $\overline{H}_{app}$ is parallel to three-fold [111]-type axes. If one defines a "mean resonance field" $H_0 \equiv h\nu/g\beta$, it can be seen that $H_{max} = H_0 + \frac{2}{3}H_a$, while $H_{min} = H_0 - H_a$, where $H_a \equiv 2K_1/M_s$ is the first order anisotropy field.

Let it now be imagined that the experimental sample comprises not a single spherical particle but an ensemble of *randomly oriented* spherical particles dispersed in a glass. In this scenario, the FMR absorption spectrum becomes a broad line "smeared" in a particular way between H_{min} and H_{max}. These "powder pattern" line shapes can in fact be calculated or generated numerically [25–28]. For the hypothetical case of zero single-crystal linewidth, the powder pattern for the example just considered (H_a positive) is represented by the sharp-featured pattern at the bottom of fig. 2a. This pattern tends to be broadened and obscured when the single crystal linewidth σ_{pp} is substantial compared to H_a (smooth curve at bottom of fig. 2a). In the usual experiment, the first derivative of the absorption is measured, as portrayed at the top of fig. 2a.

As apparent from comparing figs. 2a and 2b, the algebraic sign of the first order anisotropy constant K_1 is readily inferred from the sense of the spectral asymmetry. Similarly, the magnitude of H_a is easily determined to be approximately $\frac{2}{3}$ of the peak-to-peak derivative linewidth.

It might be noted that the "powder patterns" of figs. 2a and 2b are virtually mirror images of each other, when reflected about the vertical dash–dot line defining the mean resonance field H_0. That they are not exactly mirror twins is due to the use in fig. 2 of higher order corrections [24,26] to the resonance condition of eq. (1). Clearly these corrections are small for $H_0 = 3250$ G (X band), and they become completely negligible when $H_0 = 12\,500$ G (Ka band). It is pertinent to point out in this context that multidomain effects are not expected at the Ka band, since $12\,500$ G $\gg H_s$ for either metallic iron or magnetite. On the other hand, the effects of domain structure are observed at X-band for iron particles > 200 Å [17–19] and they are probably observed for magnetite as well (vide infra).

3. FMR spectra of terrestrial natural glasses

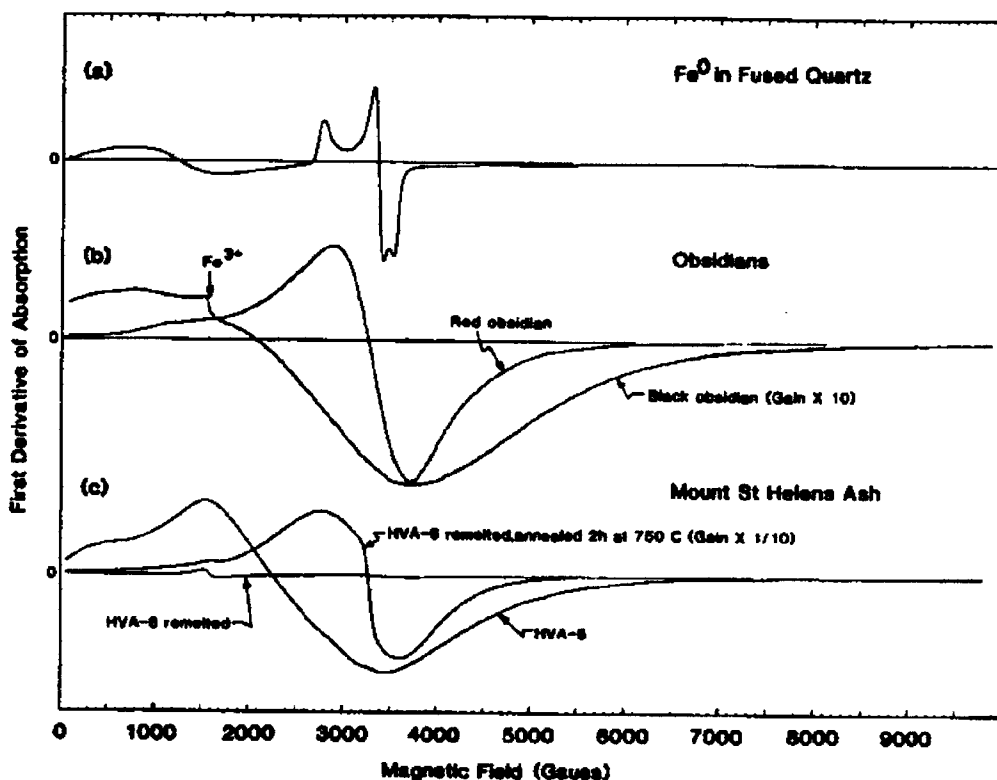Fig. 3 displays the X-band FMR spectra of some terrestrial natural glasses and one synthetic analogue.

Fig. 3. X-band (9.5 GHz) FMR spectra of fine-grained ferromagnetic precipitates in (a) synthet fused quartz, (b) obsidians, and (c) Mount St Helens ash before and after remelting ar subsequent heat treatment.

Table 1

Average chemical compositions (wt%) of rhyolitic obsidians from the western USA and of pale ar dark ash from the 18 May 1980 eruption of Mount St Helena. N.A. — not analyzed

Oxide	Obsidian [a]	Pale Ash [b] (HVA-5,6)	Dark Ash [b] (HVA-1,2)
SiO_2	76.4	68.2	64.2
Al_2O_3	13.1	16.2	17.2
Fe_2O_3	0.5	1.7	2.2
FeO	1.0	1.9	2.5
TiO_2	0.1	0.5	0.7
MnO	N.A.	0.05	0.07
CaO	0.9	3.7	5.1
MgO	0.2	1.2	1.9
K_2O	4.2	1.9	1.5
Na_2O	3.7	4.6	4.5
P_2O_5	N.A.	0.15	0.19

[a] Data from ref. [31] converted to wt%. Assignment of total iron between Fe_2O_3 and FeO w: based on Mössbauer data [31].

[b] Samples collected 5 km north of Pullman, Washington. Analyses were given in ref. [33], whei the total iron was assigned as 44% Fe_2O_3 and 56% FeO. The pale ash, which comprised 4/5 the total fallout of Pullman, was found to be 80% glass [33].

The spectrum of fig. 3a arises from spherical metallic iron particles ~ 150 Å precipitated in silica glass fused in the laboratory from natural quartz [28,29]. The sharp spectrum centered on $H_0 = 3250$ G in fig. 3a is essentially the same as the spectra observed in Fulgurites [5]. In fact, typical Fulgurite spectra have been computer simulated [30] using g value distributions and g-versus-H_a correlations virtually identical to those employed in simulating the spectra of metallic Fe:Si precipitated in fused natural quartz [28]. In this way, the physical origins of the Fulgurite spectra are confirmed.

Fig. 3b presents the FMR spectra of some obsidians from Inyo County, California. Presumably, these materials are similar in composition to an average given for 28 rhyolytic obsidian samples from California, western Nevada, and southern Oregon [31] (see table 1). Except for some nodular inclusions of crystobalite (which were excluded from the FMR experiment), the black obsidian was similar in appearance to specimens from many other locations. On the other hand, the red obsidian * exhibited a highly textured, lamellar structure, with interspersed veins of more lustrous brownish black glass (which were separated from the experimental sample). From its appearance, this red obsidian may well be an example of an obsidian sheet deposited from a fluidized flow (see discussion in ref. [1]).

The two spectra of fig. 3b are radically different from one another. From the discussion of section 2, it seems highly likely that the red obsidian spectrum is characteristic of spherical single domain ferromagnetic particles, presumably magnetite. Final verification of this suggestion must await temperature dependence studies of the types to be described in section 5. On the other hand, arguments have been developed [32] to support the hypothesis that the broad resonance with a zero-crossing near 2 kG which characterizes the black obsidian is in fact due to multidomain magnetite particles.

Part of the argument [32] for the multidomain-particle origin of such broad spectra derives from an exploratory study of Mount St Helens ash epitomized in fig. 3c. These samples are known to contain coarse-grained magnetite [33]. The spectrum of sample HVA-5 (see compositions [33] in table 1) was in large measure typical of the four ash specimens studied. Shown also in fig. 3c at the same spectrometer gain is the spectrum of a somewhat larger mass of glass prepared by fusing sample HVA-6 in a platinum crucible at 1500°C and quenching to room temperature. The loss of ESR intensity on remelting is interpreted as evidence that the ferromagnetic particles present in the as-deposited ash were redissolved into the glass.

A similar quantity of this vitrified ash was sealed in an evacuated fused quartz ampoule and annealed for various lengths of time at 700 and 750°C. The anneals at 700°C had no effect on the recorded spectra either before or after an initial nucleation of ferromagnetic phases by a $\frac{1}{2}$h anneal at 750°C. The initially narrow FMR line induced by the latter treatment broadened and

---

* Obtained from Wards Natural Science Establishment; this hand specimen was identified at the Natural Glasses Conference as a high-density welded tuff.

intensified after a total anneal time of 2 h at 750°C. The resulting spectrum, illustrated in fig. 3c is interpreted as arising from single domain particles (≤ 480 Å) of a magnetite-like phase. Futher heating at 750°C or above is expected to cause additional growth of these particles and an eventual restoration of the presumed multidomain spectrum of the as-collected ash.

As an added illustration of the potential usefullness of FMR for the study of geological materials, the mineral magnetite contents of four Mount St Helens ash samples were determined as a function of the time of their collection on the day of the ashfall (fig. 4). These samples were encapulated in precision-bore 1 mm diameter sample tubes for this measurement, and the total FMR intensities were determined by double numerical integration of the first-derivative spectra [34]. Absolute intensity calibration was by comparison with a Varian "strong pitch" standard sample, using the appropriate correction factors. It can be seen in fig. 4 that the FMR determinations of magnetite agree in their general trend with the X-ray fluorescence analyses [33] for total iron. This measurement indicates that the fraction of the total iron present as magnetite is ~ 15% for the dark ash, versus ~ 10% for the pale ash which began falling after 5 : 30 p.m.

Before turning to the subject of lunar glasses, it is fitting to comment at least briefly on those most enigmatic of all natural glasses, the tektites [1]. Simply summarized, those tektite glasses which have been investigated by ESR techniques have not exhibited easily recognizable *ferro*magnetic resonance spectra in their as-collected condition [2,5,35,36]. Rather, their spectra have resembled that of the remelted ash sample of fig. 3c, with weak *para*magnetic resonance lines due to Mn^{2+} and/or Fe^{3+} [2,5,35,36]. Ferromagnetic precipitates are apparently an uncommon occurrence in tektite glasses. Annealing
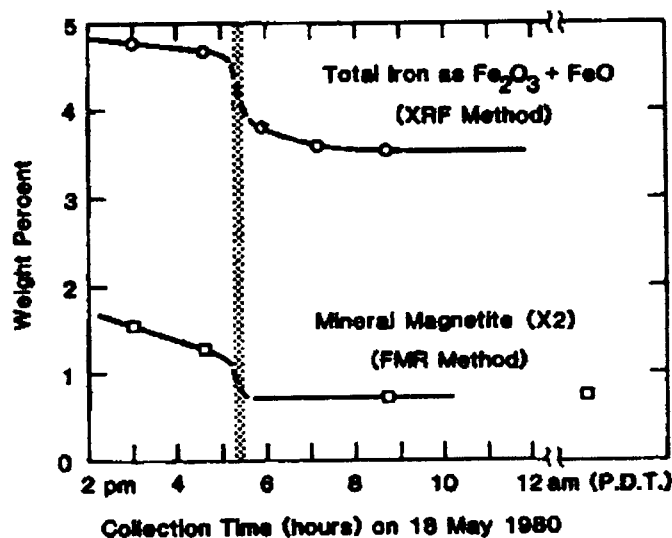

Fig. 4. Total iron and mineral magnetite contents of a series of Mount St Helens ash samples as determined by X-ray fluorescence [33] and FMR methods, respectively. Vertical band marks an abrupt change in the color of the ash from dark to pale gray [33].

tektite glasses in an oxidizing environment does, however, cause the appearance of an FMR signal [5,35] similar to that of the remelted and annealed ash sample of fig. 3a.
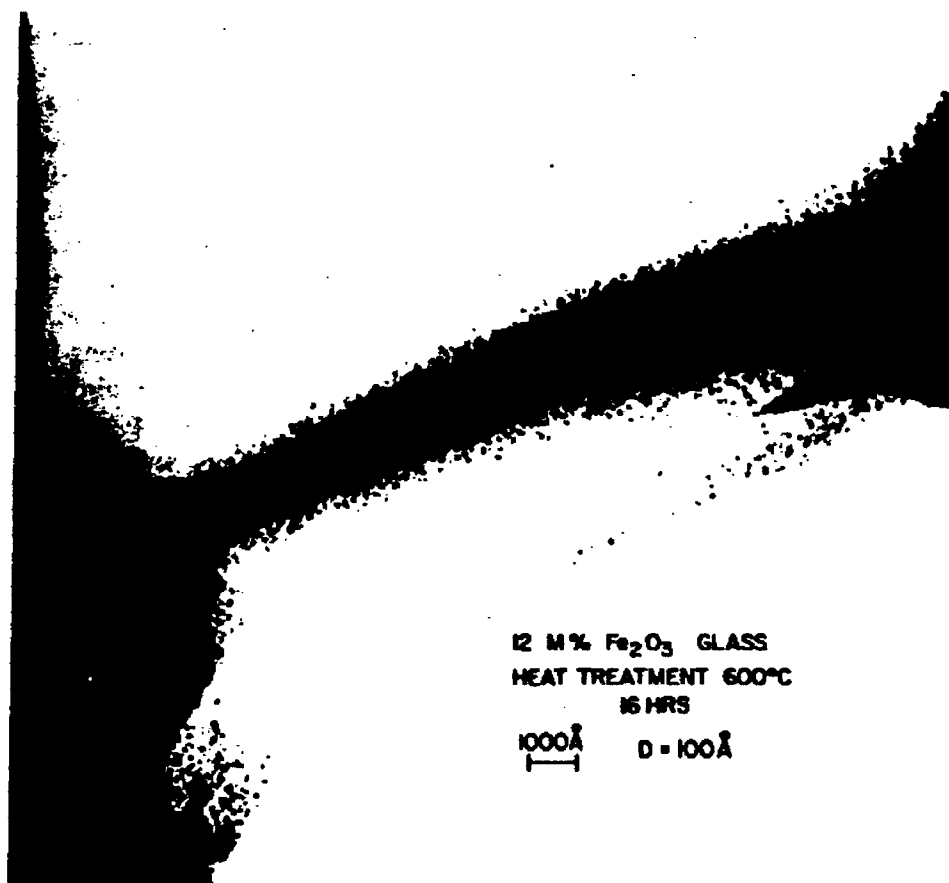
4. FMR spectra of lunar glasses and some synthetic analogues

One of the surprises coming from the first examination of the Apollo 11 lunar samples was the fact that the lunar soils comprise up to 50% glass, e.g. ref. [37]. In hindsight, this discovery should not have been as astonishing, since it was known that the Moon has been continuously bombarded throughout its history by meteorites of all sizes. It is now recognized that hypervelocity impacts by speck-sized micrometeoroids are responsible for the melting and remelting of soil particles at the lunar surface, forming a major petrological component in the soils—the glassy agglutinates. These heterogeneous cindery glass particles turn out to be rich in ferromagnetic precipitates ~ 125 Å in diameter [38] (see fig. 5a) which make the major contribution to the so-called "characteristic" FMR signal of the lunar soils [25,39–48]. However, crystalline mineral fragments and homogeneous glasses picked from the soils have also been found to exhibit FMR signals similar to the "characteristic" resonance [40,41,43,44].

It has been argued [38] that during melting by micrometeoroid impacts the lunar soil particles are chemically reduced by reaction with implanted solar wind protons. This reasoning, coupled with direct evidence of the presence of metallic iron from Mössbauer (e.g. refs. [38,49,50]) and static thermomagnetic studies (e.g. ref. [51]) led to the conclusion [38] that essentially all of the spherical particles appearing in fig. 5a are single crystals of very pure metallic iron (alloyed with at most ~ 1–2 wt% Ni [49,50]).

This "metallic iron hypothesis" for the origin of the "characteristic" resonance initially seemed to be fully supported by the FMR spectra, since the algebraic sign and magnitude of the anisotropy field H_a derived from powder pattern analysis (section 2) seemed to be right for metallic iron and wrong for magnetite [25,42]. That is, $H_a > 0$ for the "characteristic" resonance and for iron, whereas $H_a < 0$ for bulk magnetite [52]. However, a number of workers called attention to inconsistencies in the observed lunar line shapes, linewidths and intensities and their temperature dependences vis-à-vis expectation or observation for metallic iron alone (e.g., refs. [39–41,43–48]). Moreover, it was demonstrated [35,53–56] that magnetite-like * phases precipitated in glasses in fact tend to exhibit values of $H_a > 0$, contrary to the behavior of bulk

---

* The terminology "magnetite-like phases" will be used here as previously [34,45] to connote any fine-grained ferrimagnetic precipitate (containing ferric iron and presumably with spinel crystal structure) which can be produced in glass. These magnetite-like phases can differ from bulk mineral magnetite in many ways, due to, e.g. cation substitution, cation deficiency, or surface effects related to small particle sizes. As a result, unusual properties may be displayed, e.g., positive anisotropy constants.

t

b

12 M% Fe$_2$O$_3$ GLASS
HEAT TREATMENT 600°C
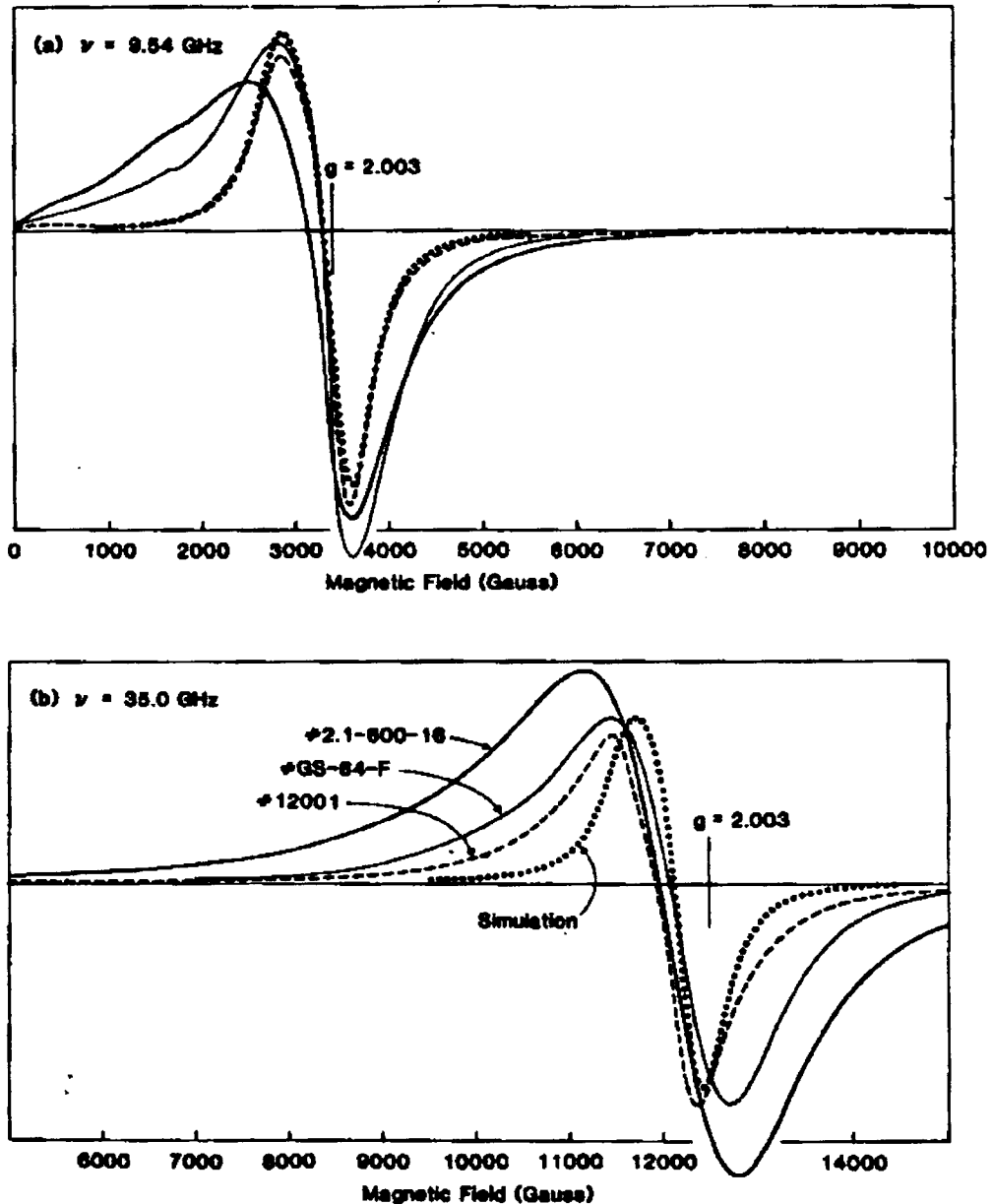16 HRS

1000Å   D = 100Å

Fig. 6. FMR spectra of a lunar soil (dashed curve) and of two synthetic glasses containing magnetite-like precipitates (unbroken curves), as obtained at X-band (a) and Ka band (b). Dotted curves are computer simulations of the lunar sample spectra using parameters previously determined [28] for metallic iron containing a few per cent silicon (see text).

Fig. 5. Transmission electron micrographs of (a) a lunar soil glass (after ref. [38]) and (b) a heat treated synthetic glass of molar composition 34% SiO_2, 25% B_2O_3, 21% CaO, 8% Al_2O_3 and 12% Fe_2O_3 with an Fe^{3+} : Fe^{2+} ratio of ≈ 2.1 (after ref. [57]). The 100 Å particles in (b) have been identified by electron diffraction as a spinel phase of lattice constant close to that of Fe_3O_4 [57].

magnetite. Finally, a comparative Mössbauer study [50] of lunar soils and samples of simulated lunar glasses containing magnetite-like precipitates, while not explicitly detecting magnetite-like phases in the lunar samples, set upper limits on the magnetite-like phases which could exist there and still escape detection. These limits, ~ 0.1–0.4 wt%, were higher than those set in ref. [49] and high enough to account for the inconsistencies alluded to above [34,45].

While the question of the origin of the "characteristic" resonance still does not appear to be resolved to the satisfaction of everyone, there seems to be adequate justification to continue to make comparisons between the FMR spectra of the lunar samples and the spectra of synthetic glasses deliberately prepared to contain only metallic iron or only magnetite-like phases. One such spectral comparison is offered in fig. 6, where the magnetite-containing samples were chosen on the basis of their extensive characterization by other techniques. (Good synthetic samples, like good lunar specimens, all have pedigrees.) Sample 2.1-600-16 is an alumino-borosilicate composition [57] (not a lunar analogue) which was particularly well characterized by electron microscopy (fig. 5b) and other techniques. Both 2.1-600-16 and GS-64-F (which *is* a lunar analogue) are more extensively described in ref. [34].

In fig. 6, the dashed curves represent the "characteristic" resonance spectra of a lunar soil sample typical of those collected from the surfaces of the lunar maria (the FMR spectra of samples collected from highland regions are somewhat narrower; see section 5). The unbroken curves in fig. 6 are spectra of magnetite-like precipitates in synthetic glasses. The latter are not necessarily "typical" of such precipitates in all cases (see, e.g., section 7) but do illustrate some widely encountered behaviors: first, it is clear from comparing the spectra of fig. 6 with those of fig. 2 that these particular magnetite-like precipitates are characterized by positive anisotropy constants ($H_a > 0$). Second, there is substantial line broadening and distortion when the spectrometer frequency is raised from ~ 9 to ~ 35 GHz. The lunar sample is also seen to exhibit similar broadening and distortion at the higher frequency.

No spectrum of a synthetic sample containing solely metallic Fe is illustrated in fig. 6, since spectra such as that of fig. 3a are too sharp to model the lunar "characteristic" resonance, while lunar analog glasses containing solely Fe° as the precipitated phase have so far tended to exhibit spectra which are distorted due to a possible multidomain component (see, e.g. ref. [34]). For this reason, the expected lineshape of single domain metallic iron is represented on fig. 6 by the dotted computer simulations. The X-band simulation employed the "corrected" powder pattern of fig. 2a, together with a distribution in H_a valves consistent with those distributions previously used successfully [28] to simulate the FMR spectra of Fe and Fe:Si in silica (similar to the spectrum of fig. 3a). Moreover, the present simulations employed the identical g-versus-H_a correlation as previously determined for Fe:Si [28]. Only a broader Lorentzian convolution function was required ($\sigma_{pp} = 360$ G, vis-a-vis 23 G for Fe:Si in silica) to achieve the excellent fit of the lunar sample spectrum seen in fig. 6a.

It bears emphasizing that previous simulations of the FMR spectra of Fe° in silica have employed the *same* parameters at Ka-band as at X-band [28]. This is to be expected for iron particles ≥ 150 Å, and the simulation of fig. 6b embodies this expectation *. Due to the poor agreement seen in fig. 6b between the simulation and the spectrum of lunar soil 12001, additional attempts were made to simulate the latter spectrum, allowing both g and H_a and their correlation to vary freely. The correct linewidth was obtained by increasing H_a by ~ 25% with respect to its mean value at X-band. However, the experimental line *shape* could not be reproduced by any combination of g and H_a values using the conventional powder pattern theory for cubic magnetocrystalline anisotropy. While the explanation for this discrepancy is still problematic, the comparison spectra of fig. 6 elicit the suggestion that some magnetite-like phases could be copresent with the fine-grained metallic iron in the lunar soils.

5. Diagnostic methods for unknown ferromagnetic phases: application to the lunar soil problem

As should be apparent from a reading of sections 3 and 4, above, FMR line shape analysis is a valuable tool for the study of natural glasses which can be used to identify unknown ferromagnetic phases (e.g., Fe° in Fulgurites) or to provide a first clue to the possible existence of unsuspected phases (e.g., magnetite-like phases in lunar soils). Since, as in the latter example, these clues will not always be accepted at face value, it becomes necessary to develop further methods for identifying unknowns. The temperature dependences of the FMR linewidth and the intensity as diagnostics for iron and magnetite have been treated theoretically as well as experimentally in ref. [29] and this source provides the basic underpinnings for the more empirical treatment of the intensity variation [34] to be summarized in the present section. Finally, some possible correlations of the "characteristic" resonance linewidth [45] and intensity [34] with the lunar soil chemistry will be examined.

Fig. 7 presents a compendium of data [28,34] for the temperature dependences of the FMR intensities of fine-grained metallic iron (a) and fine-grained magnetite-like precipitates (b) in glass, together with data for powdered natural magnetite (in b) and theoretical predictions [34,58,59] for the behaviors of large-grained iron and magnetite (dashed curves). Also shown by the upward-trending curve in fig. 7a is the behavior predicted for metallic iron particles in the limit that the particle size is much larger than skin depth δ for the penetration of the microwave field into the particle [34,59]. The latter predict-

---

* Actually, on going from 9 to 35 GHz an increase ~ 3% in H_a can be predicted [29] for particles ~ 150 Å, but such a small difference would be difficult to measure experimentally. An increase of ~ 10% would be registered for particles ~ 100 Å.
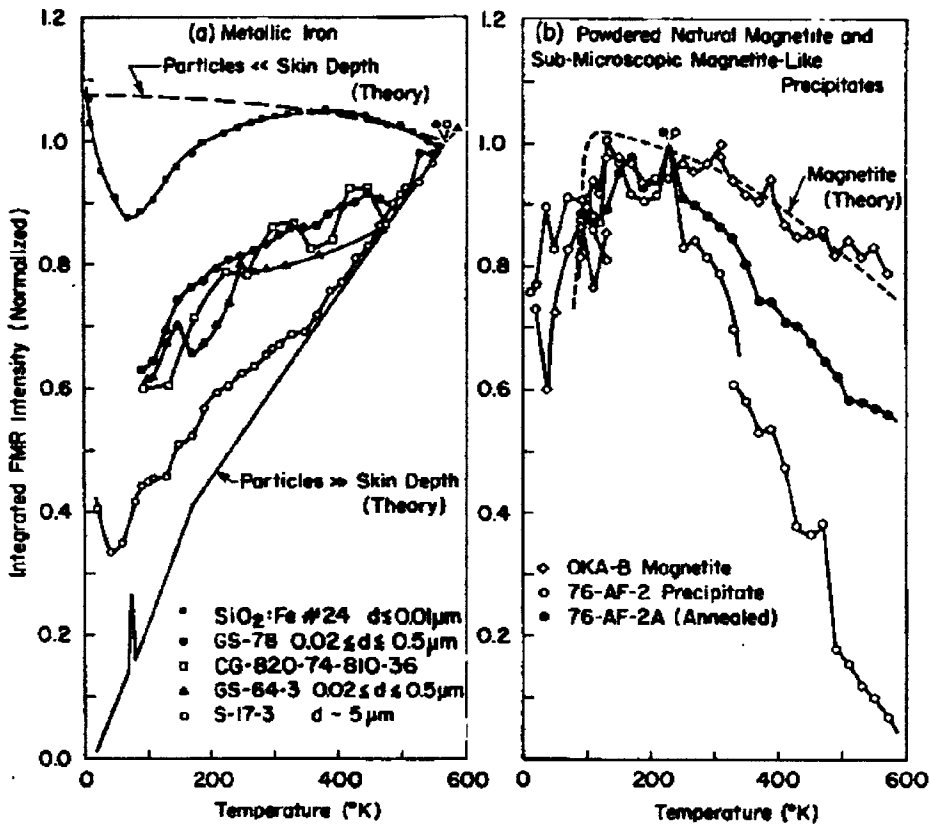
Fig. 7. Total integrated FMR intensities versus observation temperature for (a) synthetic glasses containing metallic iron precipitates and (b) powdered mineral magnetite and synthetic glasses containing magnetite-like precipitates (after refs. [28] and [34]). Additional descriptions of some of the synthetic glasses are given elsewhere in the text.

ion is governed by the premise that the observed intensity must be proportional to the saturation magnetization M_s multiplied by the fractional volume of the particle excited. For particles of diameter $d \gg \delta$, the excited volume would be proportional to $\delta = 1/(\pi \sigma \mu \nu)^{1/2}$, where (in mks units) σ is the conductivity, μ is the permeability, and ν is the microwave frequency. In point of fact, it is the temperature dependence of σ for metallic iron [60] which is responsible for the rapidly rising aspect of the curve "Particles $\gg$ Skin Depth" in fig. 7a. A series of curves of intermediate slope for values of d comparable to δ have also been presented [29].

The samples of fig. 7 are described in detail elsewhere [28,29,34]. Of particular importance have been the determinations of the particle sizes for the various iron-containing samples by means of electron microscopy, vibrating sample magnetometry, or visible light microscopy. It was on the basis of these data that the on-resonance skin depth for metallic iron at 300 K and $\nu = 9$ GHz was estimated to be ~ 50 Å [29]. The magnetite-like precipitates in the

synthetic lunar glasses were not studied by electron microscopy, but from their FMR line shapes it was readily inferred that the particles in sample 76-AF-2 were single domain ($\leq$ 480 Å), while those in 76-AF-2A were multidomain [32] ($\geq$ 480 Å). A further discussion of the latter samples will be given in section 7, below. The OKA-B magnetite was a terrestrial mineral specimen which was finely pulverized and diluted in ultrafine SiO_2. The "theory" curve for magnetite (short dashed curve in fig. 7b) includes the temperature dependence of M_s for bulk magnetite and an empirical dropoff in magnetization observed [61] below ~ 110 K in applied fields ~ 3000 G (H_0 at X-band) but neglects the microwave skin effect. Since the conductivity σ for magnetite *decreases* below room temperature [61] (in contrast to σ for metallic Fe, which increases), a slightly steeper decrease in FMR intensity between 110 and 300 K might have been predicted.

In brief summary, the data and theories of fig. 7 are in consonance with the following generalizations: (i) the FMR intensity for fine-grained metallic iron particles is an *increasing* function of temperature between ~ 50 and ~ 400 K, irrespective of particle size. The maximum intensity decrease between 400 K and 600 K expected for iron particles $\geq$ 100 Å is ~ 5% [29,34]. (ii) The FMR intensity of fine-grained magnetite (or magnetitelike precipitates) is a *decreasing* function of temperature above ~ 110 K and may exhibit sharp dropoffs just below this transition point. The finest-grained magnetite-like precipitates exhibit FMR intensity decreases approaching 100% between ~ 250 and ~ 600 K, occasionally with sharp transitions near 470 K [34].

FMR intensity-versus-temperature data for a suite of lunar soils are presented in fig. 8 [34]. Comparison * of these data with fig. 7 is striking. It can be seen that the lunar soil data are universally decreasing functions of temperature above ~ 200–300 K. The amounts of these decreases are ~ 15–35%, vis-à-vis the maximum predicted decrease ~ 5% for 100 Å iron particles. Moreover, sharp dropoffs are noted in some cases just below ~ 130 K and/or just above ~ 450 K. As recognized in the preceding paragraph, these behaviors may be indicative of fine-grained magnetite-like precipitates in glass. Assuming the presence in the lunar soils of phases with the properties of synthetic sample 76-AF-2 (fig. 7b), it would follow that metallic iron could contribute up to 85% of the single-domain resonance intensity for mare soil 12001 but at most 65% of the intensity for soil 14230 collected from the Apollo 14 landing site.

According to the "metallic iron hypothesis" [38,62] the "characteristic" resonance intensity (measured, say, at room temperature) should be simply related to the glassy agglutinate content of the lunar soils, which in turn should

---

* For reasons laid out in ref. [34], the data of fig. 8 pertain to the "narrow part" of the FMR spectrum, defined by the shaded area in the inset to fig. 9, whereas the data of fig. 7 are "total integrals." The "narrow integrals" of fig. 8 tend to include the contributions of single-domain iron and magnetite, while discriminating against multidomain iron. Since single-domain particles were the primary object of the lunar soil study, it is valid to compare the data of fig. 8 with *single-domain particle* data of fig. 7 [34].

be proportional to the length of time the sampled soil had been exposed to solar wind implantation and micrometeroid impact. Of course, in this view, the intensity would also be linearly related to the amount of Fe^{2+} in the sample available for reduction. Thus, if the "metallic iron hypothesis" were generally applicable to all lunar soils, it would be predicted that the "characteristic" resonance intensity should be directly proportional to the agglutinate content of the soil multiplied by its analyzed FeO content. Fig. 9 illustrates a test of this hypothesis presented in ref. [34]. Here it can be seen that the bar graphs representing the total FMR intensities scatter by more than a factor of two about any linear relationship one may wish to draw. No improvement is gained by considering separately the "narrow integrals" (open part of the bars) or the broader parts of the resonance (solid bars). Finally, little improvement is achieved by subtracting away the postulated contribution of magnetite-like
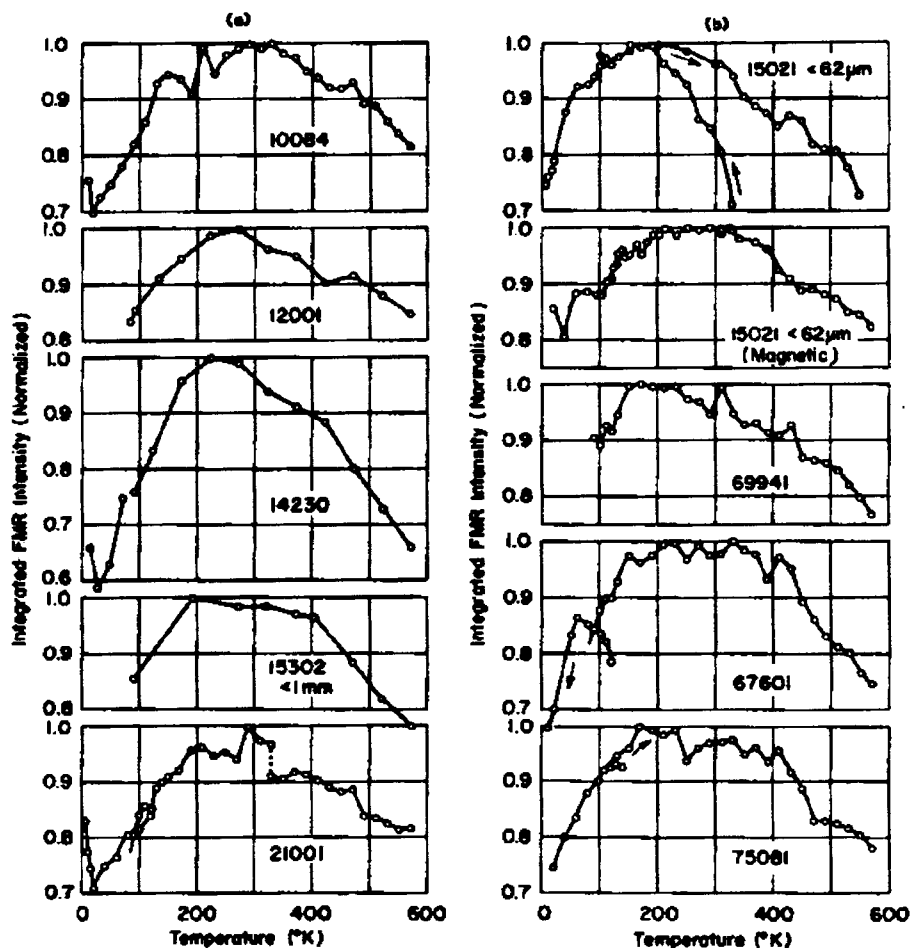

Fig. 8. FMR intensities versus observation temperature for 10 lunar soils (after ref. [34]). These data were obtained by a "narrow-integral" method which took into account only the shaded area in the inset to fig. 9 (see footnote in text).
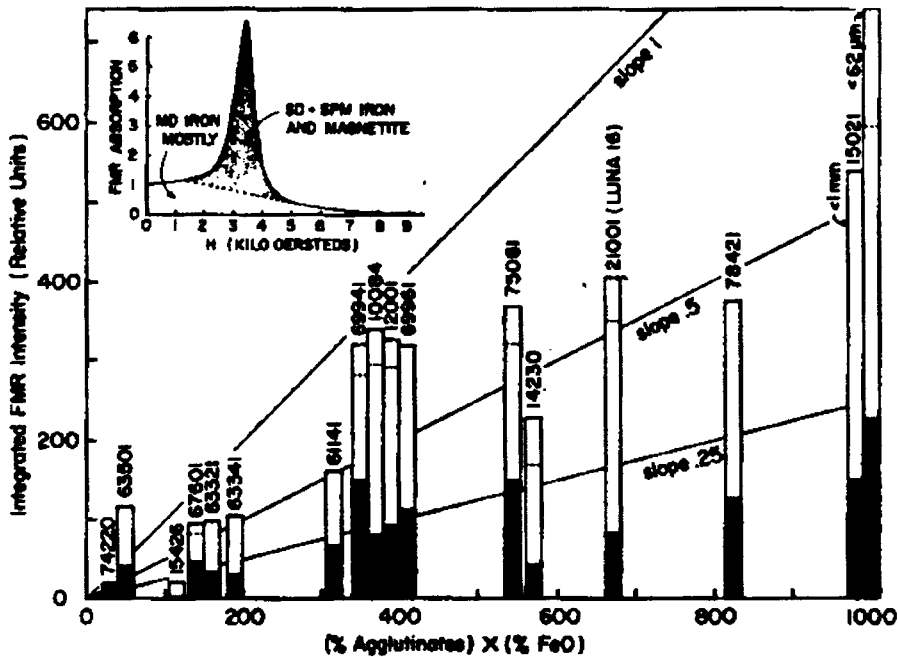
Fig. 9. Integrated FMR intensities of lunar soils versus (% agglutinate glass)×(%FeO). Total bar height represents the total area under the FMR absorption curve divided by the sample mass. Open parts of bars correspond to the narrow parts of the resonance (shaded area in inset). Bar areas above the dashed horizontal lines represent the estimated partial contribution of magnetite-like phases (see text). Bar heights are approximately convertible to wt% iron metal by dividing by 500 or to wt% magnetite by dividing by 227. The figure is slightly modified from ref. [34], where sources the chemical and physical data are cited.
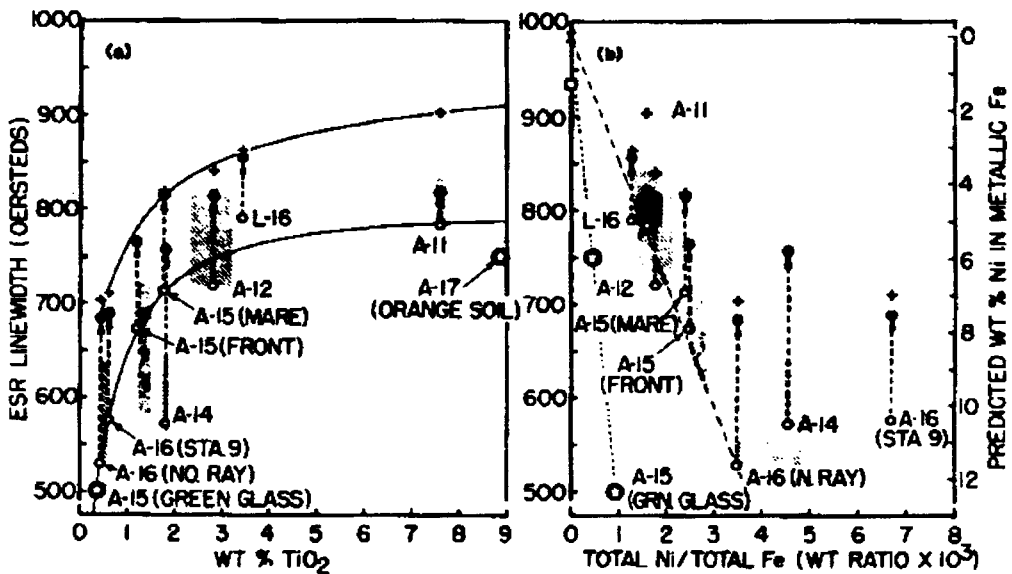

Fig. 10. Peak-to-peak FMR linewidths of the "characteristic" resonance of lunar soils plotted versus bulk soil chemistry. Meanings of the symbols and potential significances of the correlations are described in the text. The figure is slightly modified from ref. [45], where sources for most FMR and chemical data are cited. An additional Apollo 11 linewidth datum was taken from ref. [62].

phases (bar areas above dashed lines) estimated where possible from the relative amounts of magnetite-like behavior exhibited in fig. 8.

It might be noted that in both fig. 8 and fig. 9 the behaviors of the Apollo 14 samples are anomalous. Sampling error is ruled out as an explanation of the anomaly in fig. 9, since the 14230 bar graph is based on FMR measurements of 6 replicate subsamples [45] and agglutinate determinations for 2 replicate subsamples [63] from the same 5 cm thick stratum of this core sample. Rather, this "Apollo 14 soil anomaly" may conceivably be related to the unique stratigraphy of the landing site *.

The final diagnostic method to be taken up in this section involves a study of the "characteristic" resonance linewidth as a function of soil chemistry. The original idea [43] was to plot all measured FMR linewidths versus the analyzed soil compositions for each major element, plus some of the siderophile trace elements. Although the comprehensive series of plots originally envisioned were not all generated, it appeared early on [43] that a correlation with TiO_2 may have been manifested and, further, that of all correlations possible those with either titanium or nickel would have the most profound implications. In short, titanium has a natural tendency to be found in magnetites (e.g., ref. [65]), while nickel is commonly found in association with metallic iron.

Fig. 10 illustrates the results of the linewidth-versus-composition plots of ref. [45] (updated with more recent chemical data for the Apollo 15 green and Apollo 17 orange glasses). Here the shaded and hatched areas define the limits of the FMR and chemical data from all available sources. All FMR data were obtained at X-band (recall from section 4 that the linewidth increases with frequency); certain Apollo 11 data possibly obtained at Ka band and included in the original figure [45] have been deleted from fig. 10. Open circles represent individual samples in as-returned condition. Filled circles riding atop the arrowheads indicate the linewidths reached after heat treatments totalling 3190 h in evacuated, sealed silica ampoules. Crosses delimit the *maximum* linewidths achieved at earlier stages in the same heating experiment.

Fig. 10a reveals a potential correlation of "characteristic" resonance line-width with the TiO_2 contents of the lunar soils. Here, another "Apollo 14 anomaly" can be noted, but this one was found to disappear after the first 10 h of the heating experiment [43]. Aside from this thermally removed anomaly, the as-returned samples tend to define a smooth curve of linewidth-versus-wt% TiO_2, with the Apollo 15 green and Apollo 17 orange glasses forming the anchor points. Similarly, the maximum linewidths after annealing (crosses)

---

* The Fra Mauro formation is believed to be an accummulation of debris emplaced in a "base surge" or "ash flow" process triggered by the planetesimal impact which excavated the Moon's Imbrium basin about 3.8 b.y. ago (see, e.g., ref. [64]). A reoxidation of the surface materials due to the slow outgassing of the deeper-lying ash deposits is a potential explanation of the low overall FMR intensity (fig. 9) and high apparent magnetite content (fig. 8) of the 14230 soil sample. This suggestion also receives ancillary support from the work of others (see discussion and sources cited in ref. [34]).

define a roughly parallel curve. Since evidence has been educed for the presence of magnetite-like phases in the lunar orange and green homogeneous glasses (see section 7 and ref. [66]), it was argued [45] that the "titanium correlation" of fig. 10a may be evidence for the presence of a ubiquitous magnetite-like constituent in the lunar soils.

On the other hand, the "Ni–Fe correlation" of fig. 10b could be used to counterargue for a Fe:Ni origin for the "characteristic" resonance. The strength of such an argument lies in the known fact that alloying of Ni with metallic iron results in a reduction of the magnetocrystalline anisotropy constant (and hence the FMR linewidth) with an almost linear dependence on nickel content between 0 and ~ 24 at% Ni [67,68]. This dependence is the basis for affixing the right hand y-axis scale in fig. 10b, "predicted wt% Ni in metallic Fe." It could perhaps even be suggested on the basis of fig. 10b that the FMR spectra of the lunar orange and green glasses are also due to Fe:Ni, if the different slope of the linewidth-versus-Ni/Fe ratio vis-à-vis the soils were ascribed to some cryptic aspect of the processes by which these homogeneous glasses were produced. Out of context then, each side of fig. 10 thus tends to neutralize any inferences based on the other.

Returning to the context of the earlier Mössbauer (e.g., [38,49,50]) and static magnetic data (e.g., ref. [51]), it is clear that up to 1 wt% metallic iron is present in some lunar soil samples, roughly half of it in sizes $\leq$ 134 Å [38,50]. This iron undoubtedly contributes substantially to the "characteristic" resonance (although the Ni content of the *fine-grained* iron component predicted from fig. 10b is substantially higher than measured [49–51]). On the other side of the coin, the temperature dependence studies of fig. 8 are reasonably interpreted as evidence for the copresence of magnetite-like constituents in the lunar soils, while the data of fig. 9 evince yet one more inconsistency in the "metallic iron hypothesis." It is not inconceivable, then, that future studies may attach limited degrees of physical significance to *both* sides of fig. 10, in so far as the unsorted soils are concerned. However, results to be discussed in section 7 will strongly indicate a magnetite origin for the FMR spectrum of the Apollo 15 green glasses.

6. Production and stability of ferromagnetic precipitates in glass: influence of redox conditions

The valence states of iron in silicate melts depend on base glass composition, melt temperature, imposed oxygen fugacity, and the concentrations of other multivalent ions present (e.g., [7–14]). However, the dependences on composition and multivalent elements are relatively small compared to the equilibrium shifts which can be effected by changes in temperature or fugacity (e.g., ref. [14]) and can be safely neglected for purposes of the following discussion, where phase relationships for the system Fe–O will be assumed to apply to any ferrosilicate melt.

Fig. 11 is a pseudo-one-component phase diagram for the system Fe–O taken from the work of Williams and Gibson [69], who compiled their data from other sources. Similar diagrams have been developed and discussed elsewhere (see, particularly, ref. [70]). In this kind of plot, the stability fields of the condensed phases are given as functions of the temperature and oxygen partial pressure. A generic labeling scheme is employed here because the pseudo-one-component diagram gives no indication of the exact Fe/O ratios of the condensed phases; for that information one must turn to a conventional binary plot as provided e.g., in ref. [70]. For example, the binary plot is required to predict the consequences of heating a self-buffered sample containing both iron and magnetite above the transition temperature (560°C) where Wüstite becomes a stable phase. In the case of materials for which $[Fe]/[0] \gtrsim$ 0.95, the magnitite is destroyed by such a heating while the metallic iron may remain stable [70]. The experimental oxygen fugacities for a suite of lunar rocks [71] are found to lie near the iron–Wüstite buffer above 560°C (data points in fig. 11), confirming that for the lunar materials $[Fe]/[0] \gtrsim 0.95$.

Shown as broken curves in fig. 11 are some C–O gas controlled equilibria [69]. The curve labeled g pertains to a C–O mixture in equilibrium with graphite at 1 atm total pressure; the curve labeled g^h represents the results of adding hydrogen ($[H]/[0] = 2$). Finally, the curve g′ gives the C–O graphite buffer for 2000 atm total pressure. These curves represent the most reducing
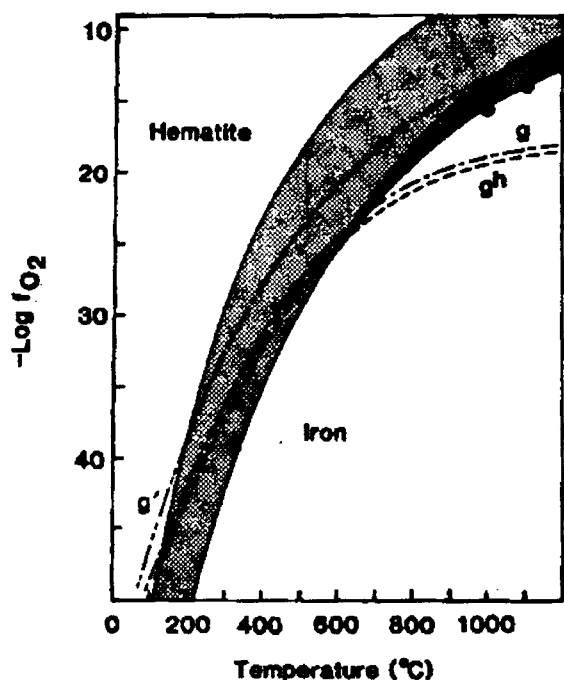

Fig. 11. Log f_{O_2} versus temperature relations for iron–oxygen buffers and for gases in equilibrium with graphite. The stability fields of magnetite and Wüstite are represented by the shaded and hatched regions, respectively. The figure is redrawn from ref. [69], where sources of the original data are cited.

gas phases possible on surface on the Moon, and the C–O equilibria may well comprise the most plausible mechanism of lunar magma reduction at depth [71], based on the gases released from lunar basalts at high temperatures (e.g. ref. [72]). Fig. 11 forcefully brings home an important point: The same gas phases responsible for the production of metallic iron in lunar rocks at high temperatures can also be responsible for the production of magnetite and other ferric oxide phases below ~ 600°C [69]. The only conceivable reason for the absence of magnetite in the lunar soils would be a kinetic barrier sufficient to stifle magnetite precipitation during all of the 600°C reheating events which have occurred in the ~ 3–4 b.y. histories of the sampled regions of the lunar surface.

It is known that magnetite (e.g. ref. [73]) and other ferrites (e.g. refs. [74–76]) can be precipitated in silicate glasses by heat treating them at a temperature T_X, which may lie ~ 50–100°C above the glass transition temperature T_g (e.g. ref. [76]). The natures of these ferrites, of course, may depend strongly on the Fe^{3+}/Fe^{2+} ratio as set by the redox conditions imposed upon melting. A ratio of $[Fe^{3+}]/[Fe^{2+}] = 2.0$ clearly favors the precipitation of magnetite (e.g., in terrestrial volcanic glasses; see section 3), whereas a glass containing ~ 100% of its iron as Fe^{2+} will not precipitate any ferromagnetic phase when heat treated in an evacuated sealed system (see below). But the same Fe^{2+}-containing glass when finely powdered and heated to the precipitation temperature T_X under controlled gas-phase buffering conditions can be made to precipitate either magnetite (e.g. ref. [53]) or metallic iron [77], depending on the imposed oxygen fugacity. Thus, *subsolidus* redox conditions can be more important in determining the magnetic phases in *finely divided* natural glasses (e.g., ash) than the conditions under which the source melt was originally equilibrated.

Fig. 12 [43,53] is illustrative of the potential for using FMR methods to follow the subsolidus production and alteration of ferromagnetic phases in glass. Simulated lunar glass GS-64 was of a composition similar to lunar "KREEP" breccias and essentially identical to that of synthetic glass GS-76 to be described in section 7, except that GS-64 contained ~ 0.1 wt% Fe^{3+} and no metallic iron [43]. It is striking that despite the availability of trace Fe^{3+} in the quenched glass no magnetic phases were precipitated after more than 200 h at 650°C in an evacuated, sealed silica ampoule (i.e., the self-buffered condition). However, 650°C is clearly near or above T_X for this material, as evidenced by the rapid initial growth of a ferrimagnetic phase when a powdered sample was annealed in air at 1 atm. Perhaps more interesting from the standpoint of interpretation is the growth curve for a third sample of GS-64 annealed in a pumped vacuum of ~ 10^{-3} atm. Here, after an incubation period of ~ 1 hour the FMR intensity grew as the $\frac{1}{3}$ power of time at 650°C. This result was interpreted [53] in terms resonance occurring in the surface layers of Fe_2O_3 particles whose volumes were growing linearly with time at temperature. Reference to fig. 11 confirms that the gas-phase buffer was indeed in the stability field for hematite.

In fig. 12, the data for lunar soil 14230 heated in an oxidizing ambient tend asymptotically to approach the corresponding curves for the synthetic glass, probably because similar processes were at work in both cases. The initial decrease in the "characteristic" resonance intensity for the lunar sample open to air at 1 atm can be ascribed to the oxidation of the fine-grained metallic iron. On the other hand, the decrease in intensity at long times for the self-buffered 14230 sample requires another explanation. Inadvertent oxidation was unlikely, since the sample was degassed at $130\,°C$ under a pumped vacuum of $\leq 10^{-6}$ Torr for 16 h before sealing the silica ampoule [43]. Rather, it has been suggested [78] that heating the self-buffered sample above $560\,°C$ results in the eventual destruction of the magnetite-like phases originally present (as predictable from fig. 11) according to the reaction

$$Fe_3O_4 + Fe^° \rightarrow 4FeO. \tag{2}$$

It should be noted, however, that the factor-of-eight decrease in FMR intensity for 14230 apparent in fig. 12 pertains only to the narrower parts of the resonance (roughly equivalent to the shaded area in the inset to fig. 9). Thus, the overall decrease in the *total* "characteristic" resonance intensity, while not yet quantified precisely, has been estimated to be $\leq 25\%$ after 1550 h at $650\,°C$ [45]. If this loss is apportioned between Fe_3O_4 and $Fe^°$ according to eq. (2), it would follow that $\sim 12.5\%$ of the "characteristic" resonance intensity (at X-band and room temperature) is due to magnetite-like phases, in general agreement with the interpretation of fig. 8 tendered above and illustrated by the dashed horizons in fig. 9.
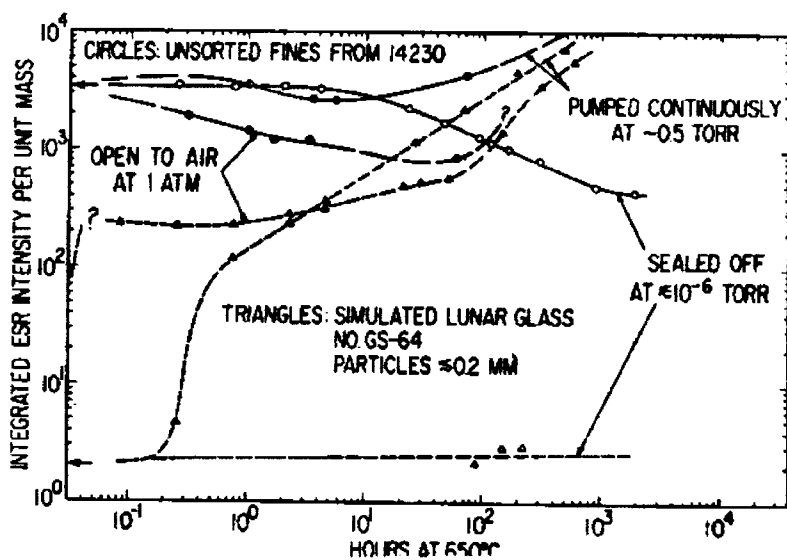

Fig. 12. The effects of isothermal anneals at $650\,°C$ in various atmospheres upon the ESR intensities of three roughly equivalent samples of Apollo 14 soil and three samples of powdered simulated lunar glass GS-64. "ESR intensity per unit mass" is expressed in arbitrary units; however, values $\geq 2 \times 10^2$ can only arise from FMR of precipitated phases. After refs. [43] and [53].

7. Laboratory simulations of ash flow chemistry and an interpretation of the FMR spectra of lunar volcanic glasses

Pai et al. [79] have described the conditions likely to prevail in a lunar ash flow. In any such process, one is dealing with small solid particles (ash or fine powder) intimately mixed with a turbulent expanding gas phase, such that the particles are "fluidized" and behave as a pseudofluid. This kind of flow could be triggered by either volcanism or impact and is a familiar phenomenon on the Earth. The differences between the terrestrial and the (hypothetical) lunar ash flow then have to do mainly with the lower gravity and lower ambient atmospheric pressure on the Moon vis-à-vis the Earth. The present section is concerned with the physicochemical effects of an ash flow process on fine particles of ferrosilicate glasses in either the lunar or the terrestrial environment. It should be evident from section 6 that the envisioned intimate gas–particle mixture should provide an ideal vehicle for investigating the influences of gas-phase equilibria on the precipitation in these glasses.

Fig. 13a is a schematic diagram of a lunar lava fountain, of the type believed responsible for the Apollo 15 green and Apollo 17 orange homogeneous glasses (e.g. refs. [80,81]). The exact nature of the gas phase present at the time of the eruption is not known. However, studies of surface correlated volitiles on the individual spherules suggest that a gas phase did exist and that it derived from a source region within the Moon different from the magma source (see, e.g., discussion in ref. [81]). It is clear that the erupting gas phase contained sulfur, but the presence of oxygen and probably carbon as well can be inferred. Thus, the phase diagram of fig. 11 is pertinent, and it can be predicted that even for a C–O gas phase in equilibrium with graphite a driving force for magnetite production would exist below $\sim 600\,°C$ (see section 6). Since the glass transition temperature for the Apollo 15 glasses was found to be $600\,°C$ [82], precipitation of some magnetite was seen to be inevitable [83], even though typical times of flight of glass particles in the eruption plume would be only ~ 40–80 s [84].

In order to test some of these predictions, a device (fig. 13b) was constructed to simulate some of the conditions present in a lunar lava fountain (or impact generated ash flow). Later models of this device [56,83] involved more elaborate plumbing for gas mixing and sampling and substituted a silica frit for the tapered throat simulating the vent from which the fluidizing gas expanded vertically into a vacuum. Of course, the force of gravity in the laboratory could not be adjusted to the lunar value, but the temperatures and pressures of the gas could be regulated in a range to model prediction for a hypothetical lunar ash flow [79]. For most experiments the initial gas temperature was $750\,°C$ and the partial pressure of water in the carrier gas (He) was deliberately varied from as low as 10^{-7} atm to as high as 3×10^{-4} atm [56]. The glass powders comprised 62–105 μm size fractions of the simulated lunar glasses whose compositions are given in table 2. Fluidization times at temperature were 2.5 h (long compared to the residency time of a spherule in a lunar
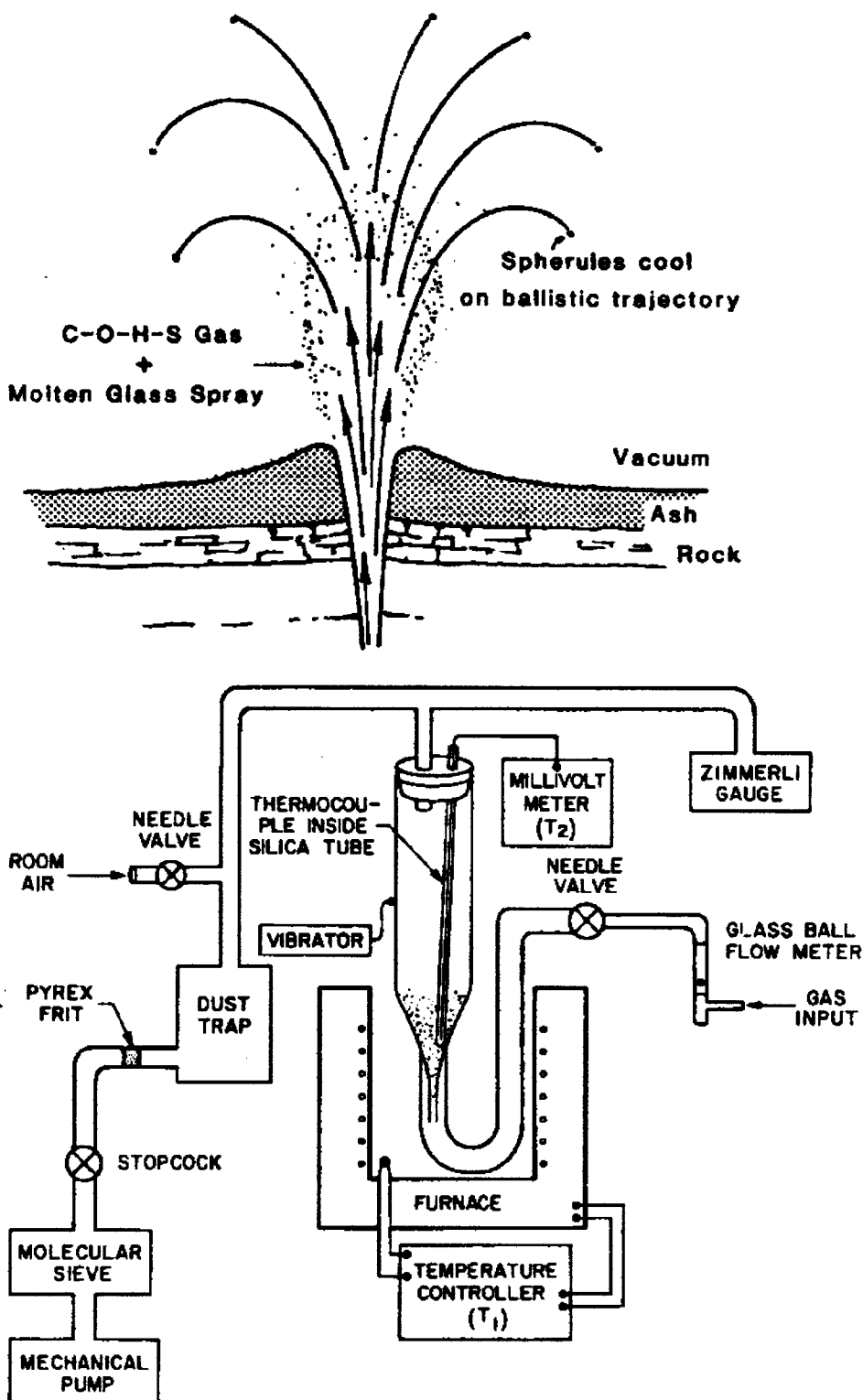
Fig. 13. Schematics of a lunar lava fountain (top) and of a laboratory device for simulating the physicochemical effects of an ash flow process (bottom).

Table 2

Compositions of several synthetic lunar glasses discussed in the text and of the Apollo 15 green glass spherules (upper entries in wt%, lower entries in ppm)

Oxide	Synthetic Glasses [a]					Apollo 15 Green Glass [b]
	CG	GS-76	GS-78	GS-79	GS-80	
SiO_2	40.4	49.8	46.2	45.2	45.2	45.3
Al_2O_3	14.5	15.5	12.4	24.9	24.9	7.6
CaO	13.3	10.4	10.6	14.9	14.9	8.5
MgO	8.1	8.4	10.4	9.2	9.2	17.4
Na_2O	0.6	0.7	0.4	0.1	0.1	0.2
K_2O	0.0	1.0	0.2	0.0	0.0	0.2
TiO_2	7.5	2.6	2.5	0.0	0.3	0.39
FeO	15.4	10.2	16.5	5.8	5.8	20.0
Fe metal	1100 [c]	2000	600	6	14	–
Fe_2O_3	N.A.	< 2	< 2	50	7	~ 70 [d]
Ti_2O_3	N.A.	3.2	< 0.1	0.2	0.3	–

[a] Glass "CG" was the base glass for CG-820-74-810-36 and is described in [77]; glasses of the "GS" series were the base glasses for the "AF" series samples described in the text; "GS" and "AF" samples are described in more detail in [34] and [56].

[b] Values are averages from ref. [81].

[c] Based on saturation magnetization of CG-820-74 [77]; all other entries on the bottom three rows are by ESR [56], cross calibrated with the metallic iron content of GS-76 as determined by static magnetization [92].

[d] Calculated on the assumption that the observed FMR signal is due to magnetite, Fe_3O_4, and that this magnetite accounts for all Fe^{3+} in the sample [45].

lava fountain, but reasonable for an ash flow triggered by a major impact).

The simulated lunar glasses of this study were melted at 1480°C and $f_{02} = 10^{-13.7}$ atm, thus matching well the redox states of actual lunar materials [71]. The ESR-FMR spectra of fig. 14a typified these materials before fluidization and were the bases for the analyses for Fe metal, Fe^{3+} and Ti^{3+} shown in table 2. It can be seen in the table that metallic iron was present in all of these samples and Ti^{3+} was small but measurable. Fe^{3+}, while measurable in the low-titanium glasses could not be detected in the higher-titanium materials [56].

The spectra of fig. 14b were those obtained for a series of samples prepared by exposing powders of glass GS-76 to "ash flow" conditions under various partial pressures of H_2O (determined by mass spectroscopy) [56]. For $P_{H_2O} = 10^{-2}$ Torr the observed spectrum due to magnetite-like precipitates is seen to be characterized by a positive anisotropy constant K_1 (compare with fig. 2) and bears a close resemblance to the "characteristic" resonance of the lunar soils (fig. 6a); this is the material denoted 76-AF-2 in fig. 7b. Lowering P_{H_2O} to 10^{-4} Torr resulted in a negative anisotropy constant, more typical of bulk magnetite [52]. While in these experiments f_{0_2} was substantially higher than might be expected for a lunar ash flow, fig. 11 suggests that the magnetite
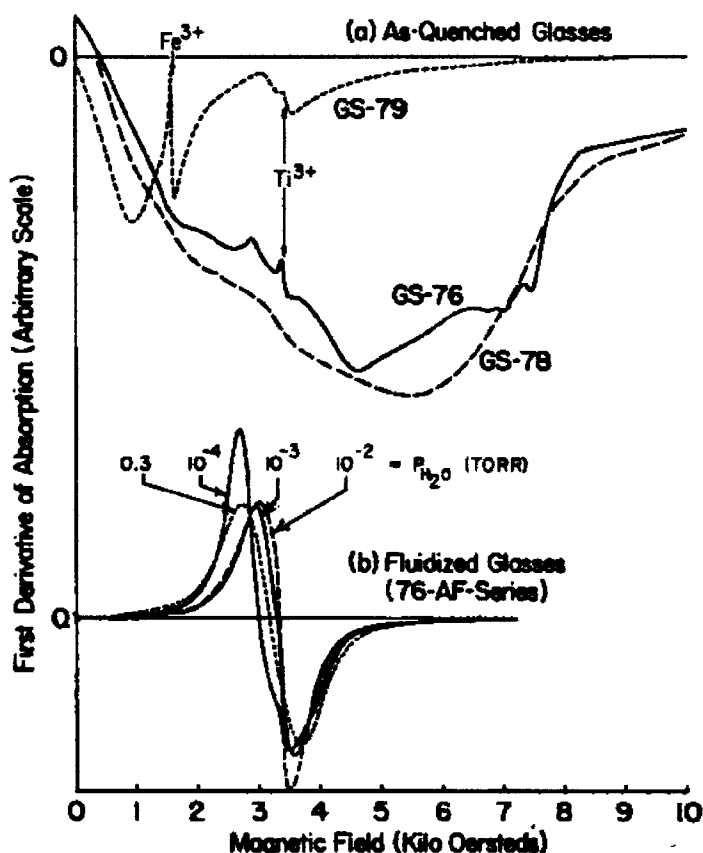
Fig. 14. ESR/FMR first-derivative spectra obtained at X-band (9 GHz) for (a) a series of as-quenched simulated lunar glasses (see table 2 for compositions) and (b) powders of glass GS-76 subjected to simulated ash flow environments. The spectra of (a) are due mainly to multidomain metallic iron and are characterized by values of (sample mass)×(spectrometer gain) ~ 500 times greater than for the spectra of (b), which are due to magnetitelike precipitates. After ref. [56].

precipitation process demonstrated here should take place even under substantially more reducing gas buffers.

Simulated lunar glasses of the Apollo 15 green glass composition (table 2) were not available at the time of these ash flow simulation experiments. However, glasses GS-79 and GS-80, roughly of Apollo 16 lunar highlands compositions, had been prepared for investigating the influence of titania content on the nature of the precipitated magnetite-like phases. These glasses were identical except for their TiO_2 contents (0%, GS-79; 0.3%, GS-80). Fig. 15 presents the temperature dependence of the FMR linewidth (a) and intensity (c) of magnetite-like precipitates produced in glasses GS-79 and GS-80 in a fluid-bed reactor similar to that of fig. 13b. It can be seen that the Ti-free sample (79-AF-1) exhibited a substantially lower linewidth at room temperature than its Ti-containing counterpart (80-AF-1), reminiscent of the TiO_2 correlation of the lunar soil spectra of fig. 10a.

The data points in fig. 15 pertain to a sample of Apollo 15 green glass
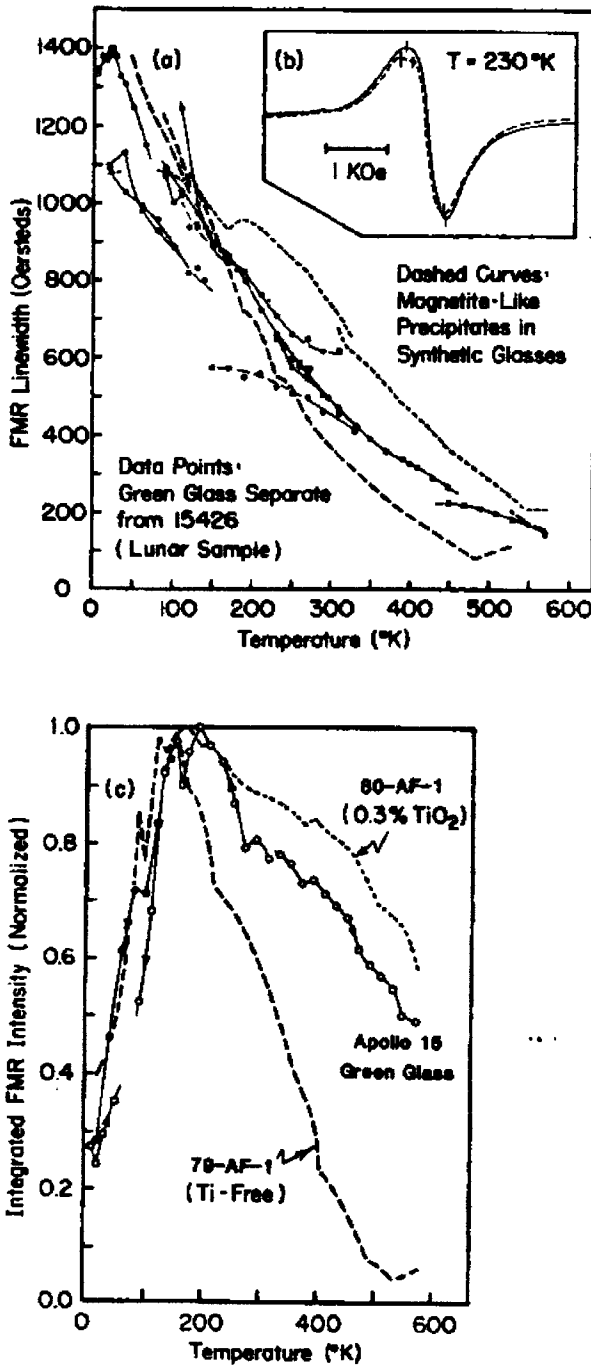
Fig. 15. FMR data versus measurement temperature (a and c) for a separate of green glass spherules from lunar sample 15426 (circles) with comparison to data for magnetite-like precipitates in two synthetic lunar glasses simulating lunar compositions (dashed curves). Open circles are data recorded before the first heating to 570 K (for reference, the temperature of lunar noon is ~ 400 K); filled circles are data obtained afterwards. Unbroken and broken curves in (b) are the lunar sample spectra respectively recorded at 230 K before and after the first heating to 570 K. Tick marks in (b) indicate the points between which linewidths were measured. After ref. [83].

spherules separated from sample 15426. It seems noteworthy that the curves for magnetite-like precipitates in synthetic "ash flow" samples 79-AF-1 and 80-AF-1 bracket the FMR data obtained from the as-returned lunar glass sample.

Two other features of the data for the Apollo 15 green glasses also point strongly to a magnetite origin for the lunar resonance signal. First, the discontinuity in the linewidth near 450 K corresponds to a reversal in spectral asymmetry at higher temperatures to be associated with a change in the sign of the magnetocrystalline anisotropy constant K_1 from positive to negative [45,55]. This kind of behavior is known in bulk titanomagnetites [85] and has been duplicated in at least one simulated lunar glass sample containing magnetite-like precipitates [86]. Second, the FMR linewidths exhibited by the Apollo 15 green glasses below 100 K become larger by $\geq 50\%$ than theoretically predicted or experimentally measured for either pure or impure metallic iron [29]. It is therefore concluded that the Apollo 15 green glass spherules contain ~ 0.01 wt% magnetite-like precipitates [45], presumably as relics of the gas-phase-imposed redox conditions which prevailed in the lunar lava fountain responsible for their creation.

8. Summary, conclusions, and recommendations for future studies

This paper has described the FMR technique as a powerful probe of the ferromagnetic precipitates which occur in a wide range of natural glasses, including Fulgurites, obsidians, terrestrial volcanic ash, lunar volcanic glasses, and lunar soil agglutinates. Other natural glasses comprising substantially more massive chunks (e.g., tektites and Lybian Desert glass [5]) have tended not to contain such precipitates, however. Sections 6 and 7 have emphasized the importance of gas-phase buffering in determining whether or not a ferromagnetic phase is precipitated and what its precise nature is likely to be. Thus, for example, the conditions present in terrestrial ash flows are seen as ideal for the precipitation of titanomagetites.

The lunar soils are known [49–51] to contain fine-grained metallic iron precipitates in quantities up to 1 wt%, and many workers have attributed the "characteristic" FMR spectra of these soils solely to this source (e.g. refs. [25,38,42,62]). However, a number of different types of FMR measurements have tended to dispute this uniformitarian "metallic iron hypothesis." First, there have been inconsistencies in the Ka-band line shape and linewidth (section 4). Then in section 5 the temperature dependence of the FMR intensity was shown to be indicative of the presence of some magnetite-like phases in addition to the more abundant metallic iron. The estimated amounts of these magnetite-like phases (~ 0.2 wt% for mature lunar soils) were revised slightly downward from refs. [34] and [45] in view of more recent data [29] for the behavior of pure iron particles ~ 150 Å in glass (data for sample #24 in fig. 7a). The presence of these amounts of magnetite, particularly in super-

paramagnetic sizes, is not inconsistent with available Mössbauer data [50,87]. Also shown in section 5 was a failed prediction of the "metallic iron hypothesis" regarding the expected [62] dependence of the "characteristic" resonance intensity on (% agglutinates) × (% FeO). Finally, a suggestive correlation between "characteristic" resonance linewidth and the titanium chemistry of the samples was pointed out (fig. 10), and the phenomenon was qualitatively replicated by magnetite-like precipitates in simulated lunar glasses (fig. 15).

If magnetite-like phases should be ubiquitous in the lunar soil glasses, their morphologies and production mechanisms must be delineated. One possibility is that they exist as thin skins or rims at the interfaces between the metallic iron particles and the glassy matrix [69]. In this case, the FMR properties of the iron particles would be perturbed by an exchange coupling with the ferrite overlayer, perhaps accounting for the line-shape peculiarities of the Apollo 12 soil in fig. 6b. Recent studies [88] of the effects of oxidations on the FMR spectra of iron wiskers might be pertinent. The possibility that some or all of these oxide layers might be due to terrestrial oxidation effects should also be considered. FMR data for metallic iron precipitates in fused silica suggest that oxide layers may develop in a period of years following sample preparation [29]. It is by no means clear, however, whether this surface oxidation of glass-encased iron is due to in-diffusion of ambient O_2 and/or H_2O or to a back reaction with water already trapped within the glass. It may be helpful to carry out comparative studies of lunar soil samples which were sealed under vacuum since their return and equivalent samples which have been exposed to the atmosphere for a number of years. This work would be best performed at Ka-band frequencies so that iron particles as small as ~ 75 Å would be magnetically saturated [29]. Also, at 35 GHz the microwave skin effect would further discriminate against the iron and thus favor observation of effects due to any ferric oxide overlayers.

Increased development and use of microwave resonance thermomagnetic analysis [34] (e.g. figs. 7 and 8) is also to be recommended. However, extreme care must be directed towards the buffering conditions present during the heating experiments, as well as the methods used to estimate the FMR intensities (see Appendix).

The issue of the magnetic phases in the lunar volcanic glasses is important in its own right and can be divorced from the general lunar soil problem. First, the nature(s) of the magnetic phase(s) in or on the Apollo 15 green and Apollo 17 orange glasses have remained cryptic [66,89]; certainly, these materials are little altered due to solar wind implantation or micrometeroid impacts. Second, the magnetite contents estimated by FMR are small (~ 0.01 wt%) for the green glass glasses themselves; by comparison, the soil "clod" 15426 from which the spherules were separated exhibited and FMR intensity ~ 10 times greater [45]. It has been suggested in section 7 that magnetite-like phases may have been precipitated in the green (and presumably the orange) lunar glass spherules as a consequence of the gas-phase equilibria present in the lunar lava fountains where they were formed.

In writing this article the author has drawn heavily on a data base, both published and unpublished, acquired with the indispensable collaboration of C.L. Marquardt and E.J. Friebele. Numerous discussions and exchanges of data with R.A. Weeks have also contributed in an inestimable way to the development of many of the ideas presented above. T. Nagata and N. Sugiura obtained the static thermomagnetic curves for sample 76-AF-2 shown in fig. 16c. In this context, it is fitting to acknowledge one more time those individuals who prepared or provided the synthetic samples so crucial to developing coherent interpretations of the natural glass spectra. The "GS" series simulated lunar glasses were melted by C.E. Schott, and the "AF" series powders were prepared from these by C.L. Marquardt using a fluid-bed reactor of his own design and construction (fig. 13 b). The "CG" glass was made available by G.W. Pearce, and the data shown were taken by R.A. Weeks. M.J. O'Horo, R.M. Housley and D.B. Shinn provided glasses 2.1-600-16, S-17-3, and FQ-24, respectively, together with important details of their characterization; fig. 5b is one of O'Horo's contributions. In the natural glass department, the Lunar Sample Curator, M.B. Duke, was extremely helpful in providing special samples under NASA Order No. T-4735A. P.R. Hooper is to be thanked for his recent gift of a pedigreed series of Mount St Helens ash samples. Finally, the author is indebted to R.J. Ginther for remelting one of the ash samples for the experiments described in section 3.

Appendix: Methods of thermomagnetic analysis

Thermomagnetic analysis is a time-proven technique for determining the nature and quantity of ferromagnetic minerals in rocks (e.g., refs. [65]). In its simplest description, the method involves measurement of the sample magnetization as a function of temperature in a fixed applied magnetic field. For high enough laboratory fields, the thermomagnetic curve so obtained consist essentially of the saturation magnetization $M_s(T)$ of the ferromagnetic mineral(s) superimposed on the paramagnetic and diamagnetic contributions of the remainder of the sample. Since the latter are generally weak in the temperature range above room temperature, the ferromagnetic mineral phases are usually identified by their Curie temperatures, the points where $M_s(T)$ falls abruptly to zero.

In practice, the situation is generally not so simple as described above. For example, indistinct Curie temperatures may be manifested either as a result of a mixture of magnetic phases characterized by a distribution of Curie temperatures [65] or as a result of the magnetic particles being too small to achieve magnetic saturation under the experimental conditions [29,90]. Furthermore, irreversible changes may be observed in the first (but not the subsequent) heating cycles, implying a phenomenon not attributable to oxidation or reduction, but rather to homogenization, exsolution, or some other internal re-equilibration [65].

Ref. [34] has attempted to lay the groundwork for an analogous technique,
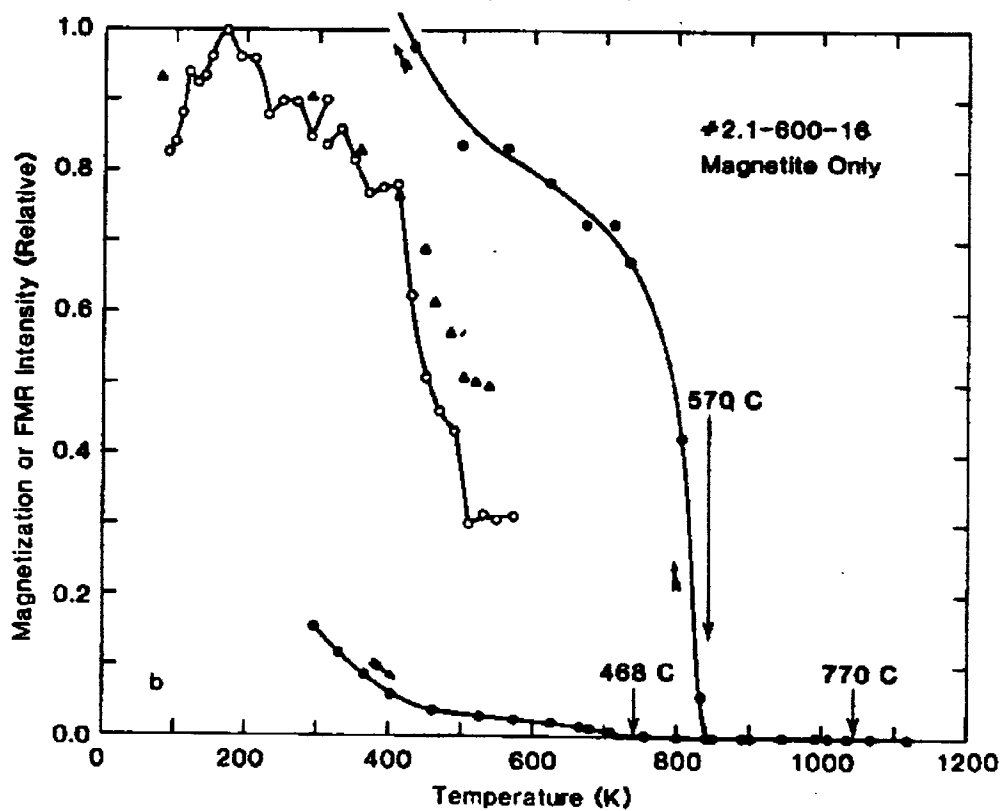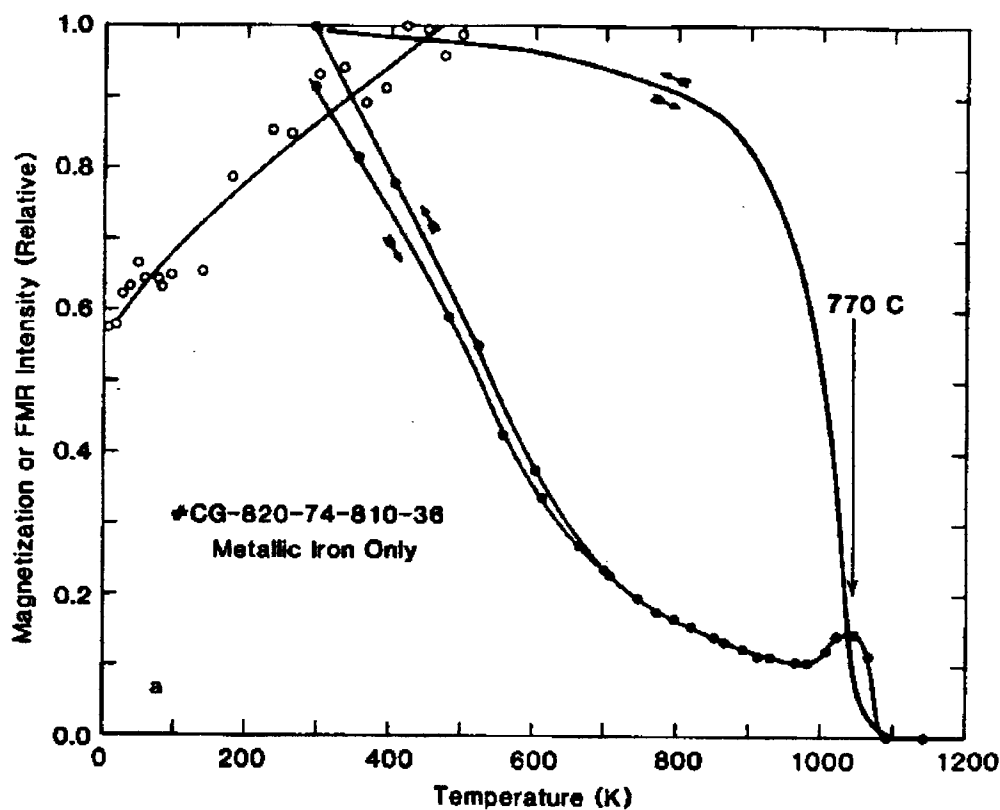
microwave resonance (or FMR) thermomagnetic analysis. The analogy between the two techniques is that each measures magnetic intensity (magnetization in the one case, FMR absorption in the other) as a function of temperature. However, the FMR method as developed in ref. [34] and epitomized in fig. 7 is capable of identifying unknown ferromagnetic phases without heating to the Curie points of the constituent ferromagnetic minerals, thus averting some of the irreversible effects eluded to above. This approach also achieves almost total discrimination against paramagnetic and diamagnetic contributions to the static susceptibility.

Others have broadened the definition of FMR thermomagnetic analysis to include measurements of any FMR spectral quantity [e.g., linewidth ΔH, peak height A_{pp}, or related quantities such as $A_{pp} (\Delta H)^2$] as a function of temperature up to and above the relevant Curie temperature(s) [91].

The purpose of this Appendix is to compare and contrast the results of various approaches to FMR thermomagnetic analysis and to relate these in turn to the results of the more classical static thermomagnetic analysis a described, e.g., in ref. [65]. For this purpose, sets of data have been compiled for all three experimental approaches, each applied in turn to the same four samples (fig. 16). For all of the FMR measurements the samples were sealed in evacuated fused quartz tubes [34,91].

Fig. 16a shows data for "CG" series glasses (table 2) which contained fine-grained metallic iron as a result of subsolidus reduction. The static magnetization curve (no data points shown) was taken from ref. [77] for a sample containing ~ 3.3 wt% iron. The filled circles pertain to data taken by the "$A_{pp}(\Delta H)^2$" FMR method [91] for CG-820-74-810-36 containing ~ 0.1 wt% iron, ~ 60% of the grains $\leq$ 150 Å [34]. The open circles [34,47] are data for another sample of CG-820-74-810-36 employing the total area (by numerical integration) under the FMR absorption curve; the upward trending character of this curve can be ascribed to the microwave skin effect (see section 5). All three methods identify metallic iron: the total-area FMR method by the skin effect and the two high-temperature measurements by the Curie point (770 °C is the Curie point for pure iron). (The peak in the FMR data near the Curie point is due to the removal of shape and multidomain anisotropy as the magnetization approaches zero [91].) Note that all three thermomagnetic curves were reversible, indicating that no oxidation, reduction, or internal reactions had occurred.

Fig. 16b shows three sets of thermomagnetic curves for a glass initially containing 100 Å magnetite precipitates [57] (see fig. 5b). Data for the total-area FMR method [43] (open circles) and static magnetization method [57] (triangles) are in excellent agreement. Transition temperatures (Curie points?) are clearly manifested in the range ~ 400–500 °C in these measurements but are less apparent in the warming curve for the "$A_{pp}(\Delta H)^2$" method [91] (filled circles). However, upon cooling from 850 °C, the latter technique exhibited a major irreversible effect: the appearance of an intense component with a Curie point of 570 °C (close to that of pure Fe_3O_4 [65]). There is

Fig. a. #CG-820-74-810-36 Metallic Iron Only, with 770 C marked.

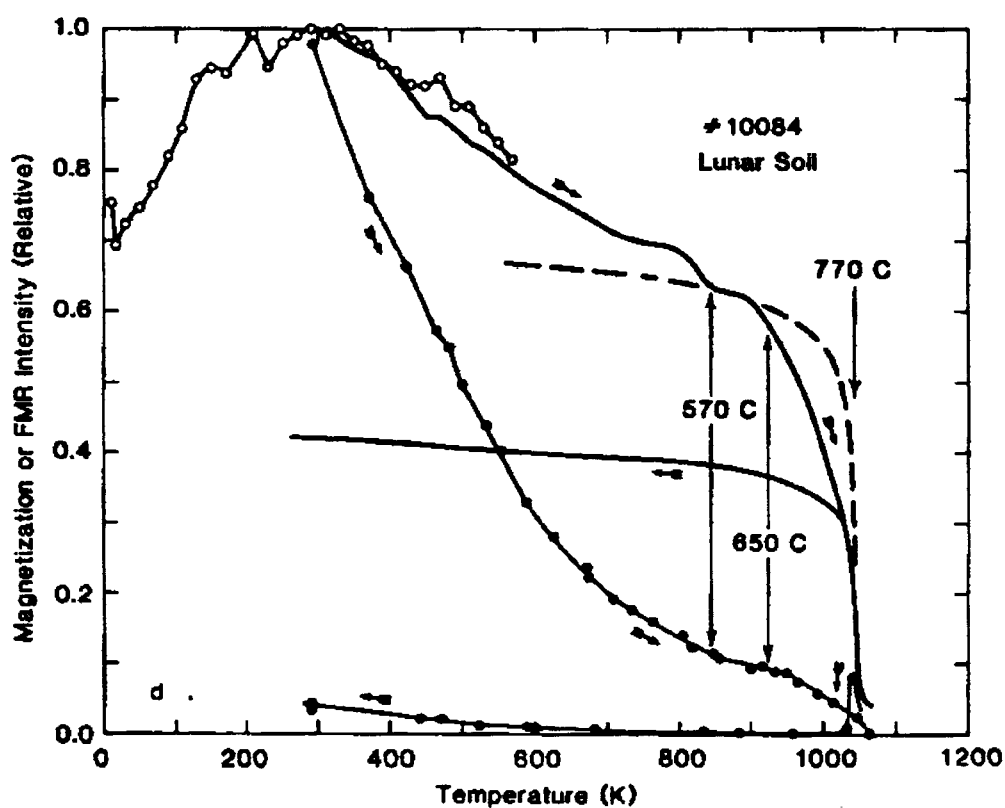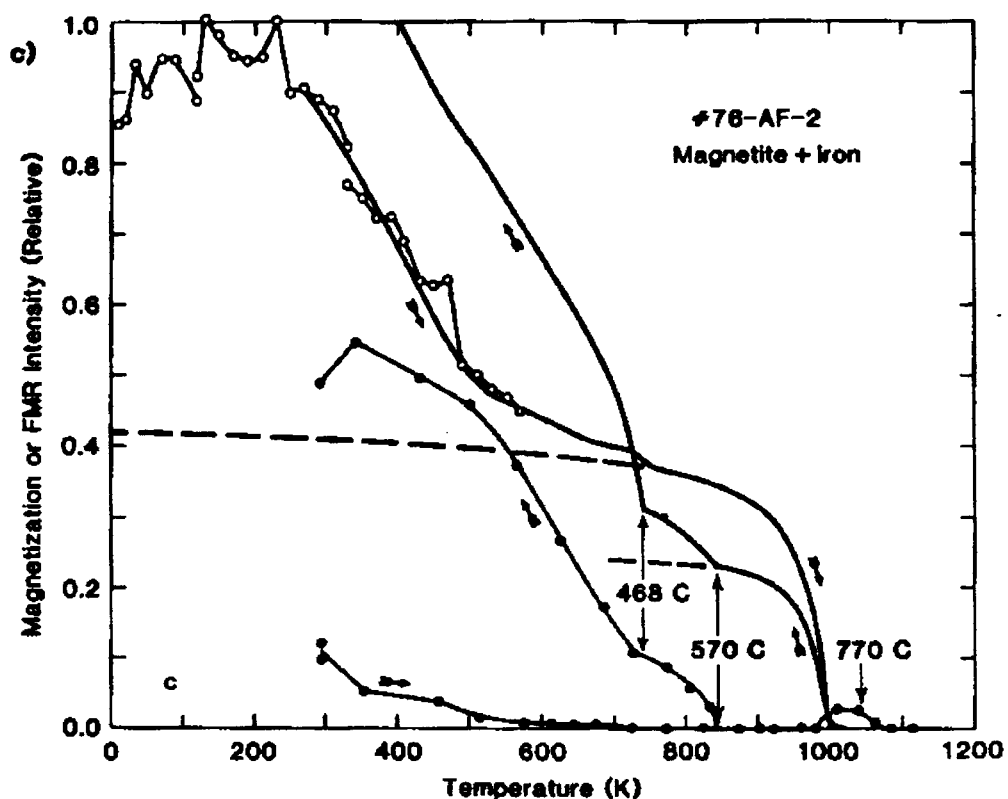Fig. b. #2.1-600-16 Magnetite Only, with 468 C, 570 C, and 770 C marked.

Fig. 16. FMR and static thermomagnetic curves for three synthetic glass samples (a, b and c) and one lunar soil (d). See text for definitions of symbols, sources of original data, and other details.

sufficient ancillary evidence [57] to conclude that this irreversible effect is due to the coarsening and further growth of the magnetite precipitates under the severe conditions of the experiment (measurements up to $850\,^\circ C$ vis-à-vis $T_x \approx 600\,^\circ C$). On the other side of the coin, these experiments show that $100\,\text{Å}$ magnetite particles do not behave like bulk magnetite; they show no Curie point at $570\,^\circ C$ but instead exhibit relatively indistinct magnetic transitions near 200 and $468\,^\circ C$.

Nagata of Sugiura [92] have carried out static thermomagnetic analyses on simulated lunar glass GS-76 (table 2) and on a simulated ash flow sample 76-AF-2 prepared therefrom (section 7). These experiments employed a laboratory magnetic field of 5.53 kG and a pumped vacuum experimental ambient ($f_{O_2} \sim 10^{-9}$ atm). The thermomagnetic curves so obtained were decomposed into a temperature-independent paramagnetic term ~ 0.035 emu/g of unknown origin, the calculated contribution $X_p(T)H$ of the known concentration of Fe^{2+} in the sample (table 2: 10.2 wt% FeO), and the contributions of the ferromagnetic phases present. For GS-76, the latter comprised essentially only metallic iron (Curie temperature $\approx 740\,^\circ C$), with a room temperature magnetization ~ 0.4 emu/g (corresponding to ~ 0.2 wt% Fe metal). The first warming curve (not illustrated) showed the presence of a minor phase (~ 0.07 emu/g) with an illdefined Curie temperature $\sim 200\,^\circ C$; upon cooling this phase had essentially vanished and the magnetization due to metallic iron had increased to $\sim 118\%$ of its initial value. Subsequent warming and cooling curves duplicated the first cooling curve. These second-run results were particularly significant in that they showed that the glass-encased metallic iron *was not oxidized* in the course of this experiment, even though the gas buffer lay in the stability field for hematite (fig. 11).

The unbroken curves without data points in fig. 16c are the static thermomagnetic curves obtained [92] under the above conditions for the "ash flow" sample 76-AF-2; the calculated paramagnetic terms have been subtracted away, however, so the illustrated curves pertain only to the ferromagnetic phases. The second warming and cooling curves (not shown) accurately replicated the first cooling curve, again indicating that no oxidation took place despite the nominally oxidizing atmosphere. The long-dashed curves in fig. 16c show the extrapolated contributions of metallic iron to the warming and cooling curves.

Comparison of fig. 16c with figs. 16a and b indicates that 76-AF-2 contained both metallic iron and fine-grained ($\sim 100\,\text{Å}$) magnetite-like phases prior to the first warming run, the magnetite being manifested as indistinct Curie points at ~ 200 and $\sim 468\,^\circ C$. The first cooling curve then shows that $\sim 40\%$ of the metallic iron was destroyed by warming above $800\,^\circ C$, while the magnetite grains were caused to grow in size as represented by the appearance for the first time of a Curie point at $570\,^\circ C$. Qualitatively, the "$A_{pp}\,(\Delta H)^2$" FMR method (filled circles) gave the same result when applied to 76-AF-2 [91]. Similarly, the presence of fine-grained magnetite-like phases was also revealed by the total-area FMR method (open circles), which was reversible in the

temperature range over which it was employed [34]. Note, a temperature independent term had to be added to the data of fig. 7b in order to bring the total-area FMR data (open circles in fig. 16c) into registration with the first warming curve of the static magnetization study. It is inferred that the total-area FMR method does not accurately reflect the metallic iron content of this sample, presumably because the particle sizes $d \sim 1000$–2000 Å [34] far exceeded the on-resonance microwave skin depth $\delta \sim 50$ Å [29]. The "$A_{pp}(\Delta H)^2$" method [91] does detect this iron as "bump" near 770°C, however.

Summarizing fig. 16c, all methods indicate (or do not contradict) the copresence of both metallic iron and magnetite-like phases in "ash flow" sample 76-AF-2. The irreversible decrease in metallic iron concentration realized on the first cooling run of the static magnetization experiment is evidently not due to gas phase oxidation (see above). Presumably this iron is destroyed by a reaction internal to the sample. A reasonable hypothesis is that the iron particles reacted with an interfacial layer of magnetite according to eq. (2) and that when this layer was consumed no further reaction took place in the time of the experiment because the iron particles were spatially isolated from the remaining magnetite in the sample.

The final case study of this Appendix involves Apollo 11 lunar soil 10084 (see fig. 16d). Here, the ferromagnetic phases should be formally regarded as "unknowns" which hopefully can be determined from the data. The static thermomagnetic curves (without data points) are taken from ref. [51]. On first warming they show a possible Curie point at 570°C (magnetite?) and a definite Curie point at 770°C due to very pure metallic iron. However, the shape of warming curve differs from prediction for iron (dashed curve) in a way that suggests that some of the iron is being destroyed above ~ 650°C. The cooling curve shows that indeed nearly half of the iron was destroyed – in addition to an unknown ferromagnetic phase with a static magnetic behavior essentially identical with the fine-grained magnetitelike phases in 76-AF-2 (fig. 16c). In contrast to 76-Af-2, however, lunar soil 10084 exhibits an irreversible *loss* in FMR intensity ["$A_{pp}(\Delta H)^2$" method] on cooling from above 800°C [91]. Morris et al. [91] ascribed this effect to an inadvertent oxidation of the iron in their sample, even though they backfilled one of their sample tubes with CO. In view of the fact that no inadvertent oxidations occurred in the synthetic samples even when exposed to a slightly oxidizing atmosphere (see above), a more reasonable explanation would seem to be an internal reaction of the iron with an interfacial oxide layer [93]. It has been suggested [93] that the residual dispute over whether or not some inadvertent oxidation occurred in the lunar soil samples could be resolved by reperforming the experiment with samples which are buffered by copious amounts of powdered metallic iron (graphite would also serve). To the author's knowledge, this suggestion has never been acted upon.

References

[1] J.A. O'Keefe, plenary lecture, these Proceedings (Natural Glasses), p. 1.
[2] R.A. Weeks et al., unpublished reports.
[3] A. Bishay and F. Hassan, in: Interaction of Radiation with Solids, ed., A. Bishay (Plenum, New York, 1965) p. 75.
[4] M. Nasrallah, S. Arafa and A. Bishay, in: Non-Crystalline Solids, ed., G.H. Frischat (Trans Tech. Aedermannsdorf, 1977) p. 148.
[5] R.A. Weeks, M. Nasrallah, S. Arafa and A. Bishay, J. Non-Crystalline Solids 38–39 (1980) 129.
[6] R.A. Weeks et al., these Proceedings (Natural Glasses) p. 593.
[7] R.V. Morris and L.A. Haskin, Geochim. Cosmochim. Acta 38 (1974) 1435.
[8] R.V. Morris, L.A. Haskin, G.M. Biggar and M.J. O'Hara, Geochim. Cosmochim. Acta 38 (1974) 1447.
[9] P.M. Bell, H.K. Mao, and R.A. Weeks, Proc. 7th Lunar Sci. Conf., Geochim. Cosmochim. Acta, Suppl. 7 (1976) 2543.
[10] H.D. Schreiber and L.A. Haskin, Proc. 7th Lunar Sci. Conf., Geochim. Cosmochim. Acta, Suppl. 7 (1976) 1221.
[11] H.D. Schreiber, Proc. 8th Lunar Sci. Conf. (1977) 1785.
[12] H.V. Lauer Jr and R.V. Morris, J. Am. Ceram. Soc. 60 (1977) 443.
[13] H.D. Schreiber, T. Thanyasiri, J.J. Lach and R.A. Legere, Phys. Chem. Glasses 19 (1978) 126.
[14] H.D. Schreiber, H.V. Lauer Jr and T. Thanyasiri, Geochim. Cosmochim. Acta 44 (1980) 1599.
[15] S.E. Haggerty, Geophys. Res. Lett. 5 (1977) 443.
[16] D.L. Griscom, J. Non-Crystalline Solids 40 (1980) 211.
[17] D.L. Griscom, J. Non-Crystalline Solids 42 (1980) 287.
[18] D.L. Griscom, to be published.
[19] D.L. Griscom, C.L. Marquardt, E.J. Friebele and D.J. Dunlop, Earth Planet. Sci. Lett. 24 (1974) 78.
[20] R.F. Butler and S.K. Banerjee, J. Geophys. Res. 80 (1975) 252.
[21] D.J. Dunlop, J. Geophys. Res. 78 (1973) 1780.
[22] A.H. Morrish, The Physical Principals of Magnetism (Wiley, New York, 1965).
[23] K.J. Standley and K.W.H. Stevens, Proc. Phys. Soc. London 69B (1956) 993.
[24] E. Schlömann, J. Phys. Chem. Solids 6 (1958) 257.
[25] F.-D. Tsay, S.I. Chan, and S.L. Manatt, Geochim. Cosmochim. Acta 35 (1971) 865.
[26] D.L. Griscom, J. Magn. Reson. 45 (1981) 81.
[27] P.C. Taylor, J.F. Baugher and H.M. Kriz, Chem. Rev. 75 (1975) 205.
[28] D.L. Griscom, E.J. Friebele and D.B. Shinn, J. Appl. Phys. 50 (1979) 2402.
[29] D.L. Griscom, IEEE Trans. on Magnetics MAG-17 (1981) 2718.
[30] D.L. Griscom, unpublished simulations of spectra obtained by R.A. Weeks.
[31] J.E. Ericson, A. Makishima, J.D. Mackenzie and R. Berger, J. Non-Crystalline Solids 17 (1975) 129.
[32] D.L. Griscom, unpublished.
[33] P.R. Hooper, I.W. Herrick, E.R. Laskowski and C.R. Knowles, Science 209 (1980) 1125.
[34] D.L. Griscom, C.L. Marquardt and E.J. Friebele, J. Geophys. Res. 80 (1975) 2935.
[35] R.A. Weeks, D.L. Griscom and P.M. Bell, Proc. 18th Ampere Congress, Nottingham (1974) p. 167.
[36] D.L. Griscom, not published.
[37] The Lunar Sample Preliminary Examination Team, Science 165 (1969) 1211.
[38] R.M. Housley, R.W. Grant and N.E. Patton, Proc. 4th Lunar Sci. Conf., Geochim. Cosmochim. Acta, Suppl. 4 (1973) 2737.
[39] R.A. Weeks, A. Chatelain, J.L. Kolopus, D. Kline and J.G. Castle, Science 167 (1970) 704.
[40] R.A. Weeks, J.L. Kolopus, D. Kline and A. Chatelain, Proc. Apollo 11 Lunar Sci. Conf., Geochim. Cosmochim. Acta, Suppl. 1 (1970) 2467.

[41] J.L. Kolopus, D. Kline, A. Chatelain and R.A. Weeks, Proc. 2nd Lunar Sci. Conf., Geochim. Cosmochim. Acta, Suppl. 2 (1971) 2501.

[42] F.D. Tsay, S.I. Chan and S.L. Manatt, Proc. 2nd Lunar Sci Conf., Geochim. Cosmochim. Acta, Suppl. 2 (1971) 2515.

[43] D.L. Griscom and C.L. Marquardt, Proc. 3rd Lunar Sci. Conf., Geochim. Cosmochim. Acta, Suppl. 3 (1972) 2397.

[44] R.A. Weeks, Proc. 3rd Lunar Sci. Conf., Geochim. Cosmochim. Acta, Suppl. 3 (1972) 2503.

[45] D.L. Griscom, E.J. Friebele and C.L. Marquardt, Proc. 4th Lunar Sci. Conf., Geochim. Cosmochim. Acta, Suppl. 4 (1973) 2709.

[46] R.A. Weeks, Proc. 4th Lunar Sci. Conf., Geochim. Cosmochim. Acta, Suppl. 4 (1973) 2763.

[47] R.A. Weeks and D. Prestel, Proc. 5th Lunar Sci. Conf., Geochim. Cosmochim. Acta, Suppl. 5 (1974) 2709.

[48] E.J. Friebele, D.L. Griscom, C.L. Marquardt and R.A. Weeks, Proc. 5th Lunar Sci. Conf., Geochim. Cosmochim. Acta, Suppl. 5 (1974) 2729.

[49] R.M. Housley, R.W. Grant and M. Abdel-Gawad, Proc. 3rd Lunar Sci Conf., Geochim. Cosmochim. Acta, Suppl. 3 (1972) 1065.

[50] D.W. Forester, Proc. 4th Lunar Sci. Conf., Geochim. Cosmochim. Acta, Suppl. 4 (1973) 2697.

[51] T. Nagata, Y. Ishikawa, H. Kinoshita, M. Kono, Y. Syono and R.M. Fisher, Proc. Apollo 11 Lunar Sci. Conf., Geochim. Cosmochim. Acta Suppl. 1 (1970) 2325.

[52] L.R. Bickford Jr, Phys. Rev. 78 (1950) 449.

[53] D.L. Griscom and C.L. Marquardt, in: Amorphous Magnetism, eds., H.O. Hooper and A.M. de Graff (Plenum, New York, 1973) p. 95.

[54] D.L. Griscom, Geochim. Cosmochim. Acta 38 (1974) 1509.

[55] D.L. Griscom, M.P. O'Horo and R.A. Weeks, Proc. Takasi Nagata Conf., eds., R.M. Fisher, M. Fuller, V.A. Schmidt, and P.J. Wasilewski (Goddard Space Flight Center, Greenbelt, 1975) p. 96.

[56] C.L. Marquardt and D.L. Griscom, The Moon 15 (1976) 15.

[57] M.P. O'Horo, unpublished data, used with permission; M.P. O'Horo, Am. Ceram. Soc. Bull. 53 (1974) 324; 356.

[58] D.L. Griscom, C.L. Marquardt and E.J. Friebele, J. Geophys. Res. 81 (1976) 6369.

[59] E.J. Friebele, D.L. Griscom and C.E. Patton, in: Amorphous Magnetism II, eds., R.A. Levy and R. Hasegawa (Plenum, New York, 1977) p. 561.

[60] C.D. Hodgeman, ed., Handbook of Chemistry and Physics (Chemical Rubber Publishing Co., Cleveland, 1956). p. 2362.

[61] C.A. Domenicali, Phys. Rev. 78 (1950) 458.

[62] R.M. Housley, E.H. Cirlin and R.W. Grant, Proc. 5th Lunar Sci. Conf., Geochim. Cosmochim. Acta, Suppl. 5 (1974) 2623.

[63] D.S. McKay, G.H. Heiken, R.M. Taylor, U.S. Clanton, D.A. Morrison and G.H. Ladle, Proc. 3rd Lunar Sci. Conf. Geochim. Cosmochim. Acta, Suppl. 3 (1972) 983.

[64] T.A. Mutch, Geology of the Moon (Princeton Univ. Press, Princeton, 1970).

[65] T. Nagata, Rock Magnetism (Maruzen, Tokyo, 1961).

[66] G.R. Olhoeft, D.W. Strangway, G.W. Pearce, A.L. Frisillo and W.A. Gose, EOS, Trans. Am. Geophys. Union 54 (1973) 601.

[67] L. Tarasov, Phys. Rev. 56 (1939) 1245.

[68] C.D. Graham Jr, J, Appl. Phys. 30 (1959) 317S.

[69] R.J. Williams and E.K. Gibson, Earth Planet. Sci. Lett. 17 (1972) 84.

[70] S.J. Schneider, in: Mechnical and Thermal Properties of Ceramics, ed., J.B. Wachtman Jr (US Govt. Printing Office, Washington, DC 1969) p. 19.

[71] M. Sato, N.L. Hickling and J.E. McLane, Proc. 4th Lunar Sci Conf. Geochim. Cosmochim. Acta Suppl. 4 (1973) 1061.

[72] C.B. Moore, C.F. Lewis, J.W. Larimer, F.M. Delles, R.C. Gooley and W. Nichiporuk. Proc. 2nd Lunar Sci. Conf., Geochim. Cosmochim. Acta, Suppl. 2 (1971) 1342.

[73] G.H. Beall and H.L. Rittler, Ceramic Bulletin 55 (1976) 579.

[74] R.R. Shaw and J.H. Heasley, J. Am. Ceram. Soc. 50 (1967) 297.

[75] D.W. Collins and L.N. Mulay, J. Am. Ceram. Soc. 53 (1970) 74.

[76] T. Komatsu, N. Soga and M. Kunugi, J. Appl. Phys. 50 (1979) 6469.

[77] G.W. Pearce, R.J. Williams and D.S. McKay, Earth Planet. Sci. Lett. 17 (1972) 95.

[78] D.L. Griscom, Proc. 6th Lunar Sci. Conf., Geochim. Cosmochim. Acta, Suppl. 6 (1975) 30£

[79] S.I. Pai, T. Hsieh and J.A. O'Keefe, J. Geophys. Res. 77 (1972) 3631.

[80] G.H. Heiken, D.S. McKay and R.W. Brown, Geochim. Cosmochim. Acta 38 (1974) 1703.

[81] J.W. Delano, Proc. 10th Lunar Planet. Sci. Conf. (1979) 275.

[82] D.R. Uhlmann, L. Klein, G. Kritchevsky and R.W. Hopper, Proc. 5th Lunar Sci. Coi Geochim. Cosmochim. Acta, Suppl. 5 (1974) 2317.

[83] D.L. Griscom, C.L. Marquardt and E.J. Friebele, Lunar Science VI, eds., J.W. Chamberla and C. Watkins (Lunar Sci. Inst., Houston, 1975) 315.

[84] T.R. McGetchin and J.W. Head, Science 180 (1973) 68.

[85] Y. Syono and Y. Ishikawa, J. Phys. Soc., Japan 19 (1964) 1752.

[86] C.L. Marquardt and D.L. Griscom, unpublished data.

[87] D.L. Griscom, C.L. Marquardt, D.W. Forester and E.J. Friebele, unpublished manuscri 1974.

[88] Z. Frait, D. Fraitova and R. Gemperle, Czech. J. Phys. B25 (1975) 906.

[89] T. Nagata, N. Sugiura, R.M. Fisher, F.C. Schwerer, M.D. Fuller and J.R. Dunn, Proc. 5 Lunar Sci. Conf., Geochim. Cosmochim. Acta, Suppl. 5 (1974) 2827.

[90] E. Kneller, Ferromagnetismus (Springer Verlag, Berlin, 1962).

[91] R.V. Morris, R.V. Gibbons and F. Hortz, Geophys. Res. Lett. 2 (1975) 461.

[92] T. Nagata and N. Sugiura, unpublished data (1974); D.L. Griscom, E.J. Friebele, C. Marquardt, N. Sugiura and T. Nagata, EOS Trans. Am. Geophys. U. 55 (1974) 329.

[93] D.L. Griscom, Geophys. Res. Lett. 3 (1976) 232.